LUMINESCENCE STUDIES in $Ca(PO_3)_2$:Eu^{3+} GLASS by LASER-INDUCED FLUORESCENCE-LINE NARROWING TECHNIQUE

By
Goro NISHIMURA

DISSERTATION IN PHYSICS

OSAKA UNIVERSITY
GRADUATE SCHOOL OF SCIENCE
DEPARTMENT OF PHYSICS
TOYONAKA, OSAKA

1989

Abstract

Rare-earth ions show narrow spectral lines even in solids, and the spectral characteristics of these lines give valuable information about the environment of the ions. The energy level scheme of the Eu^{3+} ion is simple compared with those of other rare-earth ions and the homogeneous linewidth is usually narrow. Further, since this ion has absorption and fluorescence lines in the visible region, it is very suitable for the laser-induced fluorescence experiment. This enables us to make very accurate spectral measurements. Therefore, this ion is a very useful probe for the investigation of the structure of host systems. However, the transition mechanism of the $^7F_0$–$^5D_0$ line of the Eu^{3+} ion, which has the most simple spectral structure, has not been understood well yet. In this thesis, the experimental research on the spectral properties of Eu^{3+} doped in $Ca(PO_3)_2$ glass is presented, which aims at explaining the transition mechanism of the $^7F_0$–$^5D_0$ line of the Eu^{3+} ion and also at yielding information on the local field of glassy material.

In general, the transition within the $4f^n$ configuration of a rare-earth ion is electric dipole forbidden. However, when the rare-earth ion is placed in some material, the transition is partially allowed due to the odd-parity crystal field acting on this ion. Judd and Ofelt developed a theory in which the electric dipole transition is allowed due to the mixing between the $4f^n$ states and the electronic states of the other configuration through the odd crystal-field potential. This theory explains most of the $f - f$ transitions very well, but does not explain the transition between the $J = 0$ states, since this theory employs the closure approximation.

In the present work, the fluorescence intensities and the fluorescence energies of the $^5D_0$–^7F_J transitions have been measured in detail for various energies of the excitation light within the $^7F_0$, $^7F_1 \rightarrow {}^5D_0$, $^5D_1$ absorption bands of the Eu^{3+} ion using the fluorescence line-narrowing technique. This

is one of the site-selection spectroscopic methods and is very useful especially in the case of rare-earth ions in disordered host materials. A linear relation has been found between the intensity and the energy of the narrowed fluorescence line of the $^5D_0$–$^7F_0$ transition. Further, a quadratic relation has been also found between the energies of the $^5D_0$–$^7F_0$ line and the $^5D_0$–$^7F_1(\varepsilon_0)$ line. This linear relation is explained by the mixing of other states into $^7F_0$ due to the local-field perturbation, because both the energy shift and the transition probability are proportional to the square of the mixing coefficient of the wave function. Further, since the quadratic relation indicates that the energy shift of the $^5D_0$–$^7F_1(\varepsilon_0)$ line is almost proportional to the second-order term of the crystal-field potential, it is concluded that the probability of the $^5D_0$–$^7F_0$ transition is proportional to the square of the second-order term. Therefore, the transition mechanism of the $^5D_0$–$^7F_0$ line of the Eu^{3+} ion in $Ca(PO_3)_2$ glass is ascribed to the borrowing of the intensity from the $^5D_0$–$^7F_2$ (M_J= 0) transition through the axial second-order term of the crystal-field potential.

The energy level structure, the fluorescence line shape and its width of the Eu^{3+} ion in this glass have also been studied. The level-mixing through the second-order crystal-field potential, which is so-called J-mixing effect, has been found to be significant to explain the experimental results. From the comparison between the experimental data and the theoretical result, information on the distributions of the second-order terms of the crystal-field potential has been obtained.

Contents

1 Introduction

1.1 Historical Overview

The optical spectrum of the rare-earth ion in solids, which is sometimes characterized as a very narrow atom-like spectrum, has been observed in the 1900s. This kind of atom-like spectrum is very different from that of the other transition metal ions which have the unfilled d orbital, and is considered to be appropriate to investigate the interaction between the optical center and its environment. However, in that time, since the sample purification was difficult, only the absorption and fluorescence spectra of limited samples were measured.

In the later 1920s, the quantum mechanics was systematized and one of its subjects was calculation of the energy levels of atoms and ions. Then, the energy level structure of a rare-earth ion was also one of the targets for understanding atomic energy levels. The basic theory of the atomic energy-level calculation was developed by Slater, and Condon and Shortley extended it in more detail in the 1930s[CoSh 35]. It was later systematized by Racah in the 1940s[Ra 43, Ra 49], who showed how the states of the d^n and the f^n configurations are classified by group-theoretical methods. These calculations were compared with the spectra of the free rare-earth atoms and ions and also with those of the rare-earth ions in solids. It was shown that these spectra are explained well by those theories. Further, it was clarified that the spectra of rare-earth ions in solids are very like those of the free ions.

In the 1950s, the spectrum of the rare-earth ion in solids was measured in detail, and many spectral lines were assigned. Further, the crystal field analysis was developed by Elliott and Stevens[ElSt 53], and Elliott, Judd and Runciman[ElJu 57]. One of their work was analysis of the crystal field splitting of a $Eu(C_2H_5SO_4)_3 \cdot 9H_2O$ crystal and the crystal-field parameters were obtained[Ju 59].

In the 1960s, the rare-earth ions in solids and in solutions attracted much interest as the laser material and luminous material for color television. Then, the spectra of many materials containing rare-earth ions were measured in order to obtain various optical constants for the laser material [Ch 63]. Further, in the theoretical side, several Russell-Saunders levels of the f^n configurations were calculated by Wybourne [Wy 61] and Gruber [GrCo 61], and the energies and eigen functions of the intermediate coupling states of f^5 and f^6 configurations were calculated by Wybourne[Wy 62] and Ofelt[Of 63], respectively. These treatments and results were reviewed in detail by Dieke[Di 68]. Further, in order to analyze the rare-earth energy levels in more detail, further interactions such as configuration interaction via the Coulomb interaction [RaWy 63, Ju 66], spin-spin, spin-other-orbit interactions [JuCr 68, CrCr 68], two particle correlation induced by the environment[BiNe 70] and covalent effect[JoPa 63, WaFr 67] were taken into account in the calculation of the energy levels. Then, the parameters which indicate the strength of these interactions were obtained for many samples by treating them as free parameters that are adjusted in order to reproduce the experimentally observed energy levels. On the other hand, Hatree-Fock calculation was first applied to the calculation of the energy levels of the Pr^{3+} ion by Ridley in 1961[Ri 61] and for many rare-earth ions by Freeman and Watson [FrWa 62]. In these calculations, the orders of magnitude of the parameters were correctly obtained. More detailed theoretical investigations of the energy levels have been attempted and more accurate atomic parameters are being obtained even now. However, in the experiment which does not aim at obtaining accurate atomic parameters, the experimental data are analyzed on the basis of the calculations developed in the earlier 1960s, which indeed explain the experimental data rather well. Therefore, basically, the experimental data are analyzed with neglecting the higher order interactions even now and also in this thesis.

The mechanism of the $f - f$ transition of rare-earth ions, which is parity forbidden, has also been investigated. This problem was first discussed

by Van Vleck in 1937[Va 37]. He considered that these transitions, which are forbidden by the Laporte rule, are allowed as an electric quadrupole transition, a magnetic dipole transition and an electric dipole transition induced by the level mixing through the crystalline field which does not have a center of symmetry and through the atomic vibration. Then, he estimated order of magnitude of the transition probability of each mechanism and attempted to explain the spectral lines for various rare-earth ions. In the year 1962, Judd[Ju 62] and Ofelt[Of 62] calculated the transition probabilities of the optical transition within the f^n configuration in detail for the first time. In this theory, the mixing between the $4f$ states and the high-lying states of the rare-earth ion such as $4f^{n-1}5d$ and $4f^{n-1}5g$ electronic configurations is taken into account with the closure approximation. Then, many investigators determined Judd-Ofelt parameters, which determine the electric transition probability, for various samples, and it has been confirmed that the experimental data are well explained by this theory for many samples. However, in some materials such as the Eu^{3+}-doped Y_2O_2S crystal in which the linear term of the crystal-field potential is considered to exist, the $J = 0$–$J = 0$ transition which is forbidden in the Judd-Ofelt theory is observed and sometimes is fairly intense. Many researchers have attempted to explain the mechanism of this transition. However, it has not been well explained yet.

After the laser was invented, the laser spectroscopy has been developed remarkably[Se 81]. One of the newly developed techniques is the site-selection spectroscopy such as fluorescence line narrowing (FLN) [Sz 70, Ri 72a, We 81] and hole burning (HB) [Go 74], which is often able to remove inhomogeneous broadening of the optical transitions in solids. Since the homogeneous linewidth brings fruitful information on the relaxation and dephasing, its measurement is very important to understand the dephasing dynamics of the optical centers in solids. The rare-earth ions in solids are particularly appropriate for this type of experiment, since the homogeneous width is usually very narrow compared with the inhomogeneous broadening. In fact, the homogeneous

width of the rare-earth ion has been investigated at various temperatures by many researchers with using FLN and HB techniques. In glassy systems, laser-induced FLN (LIFLN) technique was first applied to the investigation of the homogeneous width of a Eu^{3+}-doped phosphate glass by Kushida and Takushi [KuTa 75]. Then, in detailed experiments, the anomaly of the temperature dependence of the homogeneous width in the glassy matrix at low temperatures was observed [SeHu 76, AvCa 77, MoCh 81]. This anomaly can be explained by the existence of a tunneling-type of motion of optical centers between two inequivalent minima. This is so-called "two-level-system (TLS)" model firstly proposed by Anderson's group [AnHa 72], and independently by Phillips[Ph 72], who explained the thermal properties of the specific heat and the ultrasonic sound velocity in the glassy matrices. Many researchers have investigated this field, and many theories which explain these anomalies have been developed. Even now, this field is one of the important subjects for understanding dephasing process in the glassy matrices.

On the other hand, the mechanism of the excitation transfer between the optical centers in glassy matrices, which is sometimes called energy transfer or energy migration, has been investigated. In the rare-earth ions in solids, the absorption and emission processes can be treated as the single ion process fairly well. However, with increasing concentration of ions and temperature, two and more ions become to contribute the spectrum. The most important scheme is excitation transfer in which an excited ion transfers its excitation energy to another ion through several interactions such as dipole-dipole and electron-phonon interactions. The investigation of the excitation transfer brings fruitful information about these interactions. In glass systems, the excitation transfer was investigated as soon as the fluorescence-line narrowing was discovered [DeKi 67]. In these investigations, time-resolved fluorescence-line narrowing technique is very useful because transfer process can be observed directly. This type of experiment was first applied to a Eu^{3+}-doped phosphate glass by Motegi and Shionoya[MoSh 73]. They concluded that the phonon-assisted

transfer was the probable transfer mechanism in that glass. Further, in the Eu^{3+}-doped glass, Alimov et.al. also investigated the energy transfer mechanism from the analysis of the line broadening of the laser-induced fluorescence line [AlBa 77].

In the application side, the investigation of the energy transfer is very important to develop efficient laser materials. Since the $f - f$ transition of a rare-earth ion is very weak due to the parity selection rule, the excitation efficiency is low when the rare-earth ions are pumped optically. Therefore, many researchers have considered to pump the rare-earth ions through the energy transfer from the other activated ions which are more efficient for optical pumping. These investigations were reviewed by Reisfeld [Re 76] who analyzed the excitation spectrum and estimated transfer rate in several glasses containing rare-earth ions [ReLi 76].

The structure of the glassy matrices has been also studied by using FLN technique. The Eu^{3+}-doped glasses have been investigated in order to yield structural information of glasses since old time, because the Eu^{3+} ion has a very simple spectral structure in the visible region. After the laser was invented, glasses doped with other rare-earth ions, particularly Nd^{3+}-doped glass, have been investigated for the purpose of developing laser materials. Before the FLN technique was introduced, researchers analyzed the absorption and emission spectra of glass samples by comparing them with those of the crystals [To 39, RiDe 69]. The intensity ratio and the peak position of the spectral lines of the glass were also investigated for various glass composition [KuGa 63, GaKu 65]. After the FLN technique which usually eliminates inhomogeneous broadening was introduced, it became possible to observe the sites in glasses directly. Then, the energies of the FLN lines have been measured and the crystal-field parameters have been obtained under various excitation energies. Particularly, Brecher and Riseberg analyzed the narrowed laser-induced fluorescence lines of the Eu^{3+}-doped oxide glasses in detail, and explained the results by the ninefold coordination model [BrRi 76, BrRi 80].

It is important point of their results that there is a local symmetry of the surrounding ions even in glass systems. Further, Brawer and Weber calculated the crystal-field parameters assuming the point charge Coulomb interaction between the ligand ions and Eu^{3+} ion in glass using Monte Carlo molecular dynamics method. The FLN spectrum was reproduced rather well by the simulation of the site-to-site variation of the crystal-field [BrWe 80, WeBr 82]. These investigations were reviewed by Yen[Ye 86].

1.2 Fluorescence Line Narrowing

As mentioned above, the laser spectroscopy has been remarkably developed after the laser invention. The properties of the laser are characterized as a monochromatic and coherent light source with high power density. By using these properties, the inhomogeneity of the spectrum of the optical centers can be removed while the homogeneous spectrum can be measured in frequency and time domains. These spectroscopic techniques were reviewed by Selzer [Se 81]. In this section, FLN which is one of the site-selection spectroscopies, will be briefly reviewed.

The spectrum of the rare-earth ion in crystals is usually narrow, since the interaction between the $4f$ electrons and the external field is very weak. However, the optical spectrum in glassy matrices is broadened because of the site-to-site variation of the local-field. From the linewidth of the spectrum in crystals, the homogeneous width, which is determined by the natural lifetime and the dephasing through the interactions between the optical center and its surrounding ions, is considered to be very narrow compared with the site-to-site variation of the transition energy. Therefore, the broadened spectrum in glasses must be composed of narrow lines due to the individual ion whose center energy is widely distributed, as in Fig.1.1(a). Under the monochromatic light excitation, the subset of ions in resonance with the excitation light are excited, as in Fig.1.1(b). If the selected sites are not diffused in observation time, only

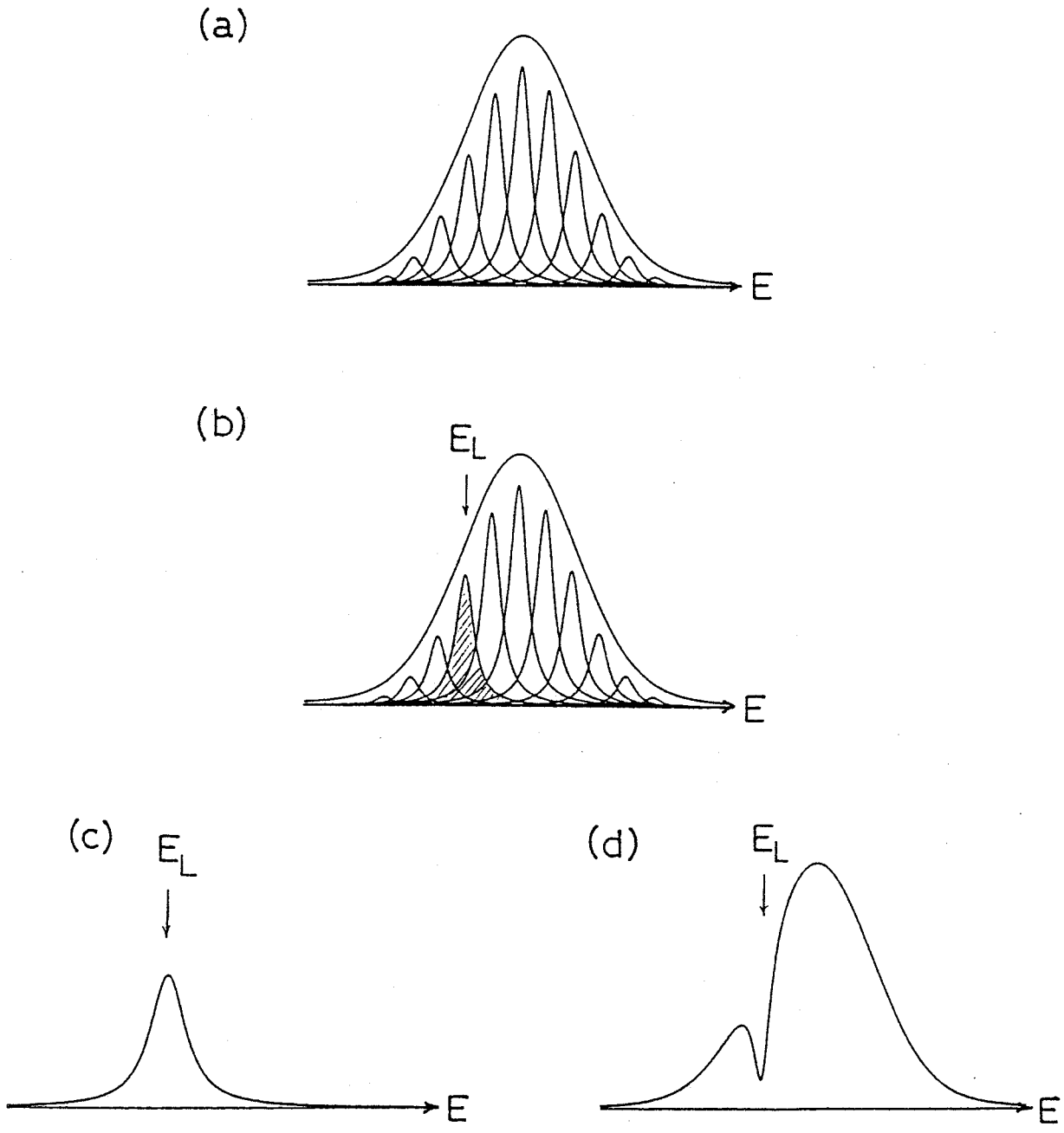

Figure 1.1: (a):Schematic representation of the inhomogeneous broadening which is superposition of the narrow individual homogeneous line shapes. (b):the monochromatic light excitation at E_L which selects the subset of the site in the inhomogeneous line. (c):the narrowed fluorescence line shape. (d):the burnt absorption spectrum.

the selected ions contribute to the emission spectrum. When the homogeneous width of the emission line is narrower than the inhomogeneous width, the observed emission spectrum is narrowed compared with the case under the broad band excitation. This is shown in Fig.1.1(c) which is so-called fluorescence line narrowing (FLN) effect. On the other hand, under the intense monochromatic light excitation, since the ground state population decreases with the pumping, the absorption is saturated. Therefore, the spectral hole is observed in the absorption spectrum as in Fig.1.1(d) which is so-called hole burning (HB) effect. These effects permit the investigation of the spectral shape of the optical transitions of the rare-earth ions in solids with the removal of the inhomogeneous broadening. Therefore, these effects are appropriate for the investigations of the homogeneous width, energy transfer, site structure and so on in amorphous solids. The FLN technique is usually a very sensitive method. However, the spectral resolution is limited by the monochromator for detection. Further, under the resonant excitation, the scattered light disturbs the detection. On the other hand, the HB technique is able to measure the spectrum with high resolution which is limited by the spectral width of the burning and probing light. However, in this case, high-intensity monochromatic light source is needed, particularly, for the rare-earth ions whose absorption coefficient is usually small. Further, because the detection of the HB is not zero method, the highly sensitive measurement is possible only with special devices for the detection.

The FLN effect in solids was found by Denisov in 1967 [DeKi 67], for the first time. He reported the FLN of the $^5D_0$–$^7F_0$ emission of a Eu^{3+}-doped borate glass with a mercury lamp excitation. After the laser was invented, the FLN experiment was applied to remove the Doppler broadening of the gas [FeJa 69]. In the optical center in solids, Szabo first applied this technique to a ruby as an analogy of the gaseous system[Sz 70]. Further, Riseberg first applied laser induced FLN technique for the rare-earth-doped glass, that is Nd^{3+}-doped glass [Ri 72a, Ri 72b, Ri 73]. He observed the nonresonant FLN

of a Nd^{3+} ion in a silicate glass with a fixed-wavelength cw laser excitation.

Next, we discuss a FLN spectrum. Let us consider an inhomogeneously broadened absorption line in solids whose spectral shape is written

$$S_{abs}(E) = \int g(E_1) f_{abs}(E_1, E)\, dE_1 \ , \tag{1-1}$$

where $f_{abs}(E_1, E)$ is the homogeneous line shape of the absorption line, and $g(E_1)$ is the statistical distribution function of the center energy E_1. If the sample is excited with monochromatic light at the energy E_L within the absorption line, a distribution of excited states is expressed as $g(E_1) f_{abs}(E_1, E_L)$. If the spectral diffusion and the saturation of the absorption are negligible, the spectral shape of the emission line is expressed as

$$F(E) = \int f_{em}(E, E_1)\, g(E_1) f_{abs}(E_1, E_L)\, dE_1 \ , \tag{1-2}$$

where $f_{em}(E, E_1)$ is the homogeneous line shape of the emission line. The homogeneous width of the zero-phonon line at low temperatures is usually narrow compared with the inhomogeneous width in the rare-earth systems, while the phonon sideband is generally broad and weak. Therefore, significant contribution for the emission line shape comes from the zero-phonon line. When we observe the emission line in resonance under the monochromatic excitation, $F(E)$ reduces to a Lorentzian with the width $2\Delta E_h$ [KuTa 75] under the assumption f_{abs} is a Lorentzian with the width ΔE_h which is much narrower than the inhomogeneous width. On the other hand, if the homogeneous width is larger than the inhomogeneous width, two Lorentzians change slightly in the region of interest and f_{abs} can be regarded almost constant. Thus, the integral in Eq.(1-2) lead to a convolution of a Gaussian and a Lorentzian, i.e., a Voigt profile. Therefore, in this case, the homogeneous width can be obtained from the deconvolution of a Voigt profile of the observed spectrum. Of course, if the homogeneous width is very large compared with the inhomogeneous one, the emission spectrum gives almost the homogeneous line shape f_{em}. Further, if both widths are of the same order, there are no suitable approximation of the integral in Eq.(1-2) and a numerical calculation is needed [HeBr 80].

In the non-resonant excitation case, the crystal-field dependence of the energy of the emission line is generally different from that of the absorption line. Then, the observed emission line is usually considered to be also broadened inhomogeneously. In this case, Eq.(1-2) should be extended and the integral with respect to the site energy E_1 should be substituted for the multiple integrals with respect to the crystal-field parameters which determine the transition energy. These will be discussed in detail in Sec.5.3.

1.3 Characteristics of the Eu^{3+} ion

The europium (Eu) is the rarest product of the rare-earth elements except promethium. In the Eu compound, the divalent or trivalent ion is stable. The divalent ion (Eu^{2+}) has an intense broad blue fluorescence due to the $d-f$ transition, though the trivalent ion (Eu^{3+}) has narrow fluorescence lines in the visible due to the $f-f$ transition. In the spectroscopic research, the trivalent ion is very interesting because of its narrow spectral lines.

In the Eu^{3+} ion, the electronic configuration is $4f^6 5s^2 5p^6$. The total number of the Russell-Saunders states is 295 and the ground state is ^7F. These Russell-Saunders states are split into J-multiplets due to the spin-orbit coupling. Several low-lying states are shown in Fig.1.2. The $^7F_0$,$^7F_1$,$^7F_2$–$^5D_0$,$^5D_1$,$^5D_2$ transitions are the optical transitions in the visible region. The fluorescent transitions originated from the $^5D_0$ state have rather simple spectral structure because the manifolds with low total angular momenta are concerned with these transitions. Therefore, the assignment of the absorption and fluorescence spectra is rather easy, and detailed theoretical analysis of the spectrum can be made also rather easily.

As mentioned above, the mechanism of the $^5D_0$–$^7F_0$ transition, which has the simplest spectral structure, has not been explained completely. This transition mechanism was proposed by several investigators. One of these mechanisms is the level mixing between the J-multiplets. In this mechanism, the

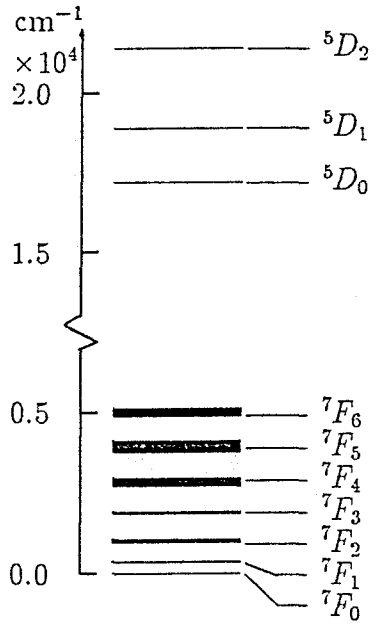

Figure 1.2: Energy Level Scheme of an Eu^{3+} ion

$^5D_0$–$^7F_0$ line borrows intensities from the $^5D_0$–$^7F_2$ and $^5D_2$–$^7F_0$ transition. Usually, however, this mechanism has been considered negligible. The second mechanism is due to the mixing of high-lying states which are not concerned in the Judd-Ofelt theory. In the Eu^{3+} ion, the energies of the $4f^5 5d$ and $4f^5 5g$ states, which are taken into account in the Judd-Ofelt theory, are higher than that of the charge transfer state (CTS) which is the hole binding $4f^6$ state [JoPa 64]. For example, the analysis in which the CTS interaction is taken into account has been investigated on a Y_2O_2S:Eu^{3+} crystal [HoIm 77]. The $^5D_0$–$^7F_1$ transition is magnetic dipole transition. The $^7F_1$ manifold is partially or fully split due to the crystal-field interaction in the case of low site symmetry. However, the transition intensities are considered to be insensitive to the crystal-field strength. On the other hand, the spectral structure of the $^5D_0$–$^7F_2$ transition is very sensitive to the environment, i.e., "hyper sensitive" transition. This is considered to come from its selection rule.

In chemical side, the halide except fluoride, nitrate, perchlorate and so on of the Eu^{3+} are soluble in water, while carbonate, phosphate and so on are insoluble. The chloride, nitrate and so on are also soluble in methanol and ethanol. Further, the Eu^{3+} ion in solution forms various stable complexes. Then, the spectra of various solutions have been measured by many researchers for investigation of the interaction between the trivalent rare-earth ion and its ligands. Because the ionic radius of the Eu^{3+} ion (0.95Å) is nearly equal to that of the Ca^{2+} ion, the local environment of the Ca^{2+} site of protein and so on can be investigated with the substitution of Ca^{2+} site by Eu^{3+}. On the other hand, the Eu^{3+} ion can be doped in various glasses such as borate, silicate, phosphate, fluoroberyllate and so on. Then, the spectra of the Eu^{3+} in various glasses have been investigated for the purpose of studying properties of the homogeneous width in the glass systems, energy transfer, local structures in the amorphous solids and also of developing new laser materials and fluorescent materials.

The $^5D_0$–$^7F_0$ transition usually has a very narrow homogeneous width, and the homogeneous width of the $^5D_0$–$^7F_1$ transitions are also narrow at low temperatures. Further, experimentally, the energies of the $^7F_0, ^7F_1 \rightarrow ^5D_0$ and $^7F_0, ^7F_1 \rightarrow ^5D_1$ transitions match with the energies of the rhodamine 6G dye laser and the coumarin 535 or 540 dye laser pumped by an Ar^+ ion laser, respectively. Therefore, the Eu^{3+} is suitable for the laser-induced fluorescence experiment. Further, because of the simple spectral structure, the Eu^{3+} ion is the most appropriate probe for the investigation of the amorphous solids. Indeed, as mentioned above, many researchers have investigated Eu^{3+}-doped amorphous solids for various aims.

1.4 Aims and Contents of This Thesis

As mentioned before, in the rare-earth-doped glass, the optical spectra due to the $f - f$ transitions are rather broad because of site-to-site variation

in the local field acting on the ions, although their homogeneous widths are usually very narrow at low temperatures. It has been considered that these spectra are not useful for the study of glass properties on account of the broad spectral widths. However, the inhomogeneous broadening can be often eliminated or reduced by the site-selection techniques such as the laser-induced fluorescence-line narrowing. Then, these techniques are considered to give much information about disordered systems which is difficult to obtain by usual methods.

Because the optical spectrum of the Eu^{3+} ion in the visible region has very simple structure compared with those of other rare-earth ions, it is most appropriate for the investigation of the local structure in solids. Therefore, many researchers have investigated Eu^{3+} contained in crystals and glasses. However, the mechanism of the $^5D_0$–$^7F_0$ transition has not been explained well yet. Then, first, we aim at explaining its mechanism in this thesis.

Recently, for the development of the tunable solid state laser material, detailed information about static and dynamic properties of the optical center in glass is needed. Especially, the investigation of the rare-earth-doped glass is important. Therefore, we aim at demonstrating a method to yield information on the local field of glass matrix with laser-induced fluorescence-line narrowing technique.

For these aims, in this thesis, the experimental research on the spectral properties of Eu^{3+} in $Ca(PO_3)_2$ glass is presented, using the laser-induced fluorescence-line narrowing technique[NiKu 88, KuNi 88].

The contents of this doctoral thesis are as follows.

Chapter 2 deals with the theoretical side of the energy levels and the transition mechanism of the $^7F_0$–$^5D_0$ line of the Eu^{3+} ion in a crystal-field. The crystal-field theory is reviewed and the energy levels and the transition probability of the Eu^{3+} ion are calculated.

Chapters 3–5 are the experimental part. In Chap.3, the experimental procedures including samples and the method of the measurement are described.

In Chap.4, the results on $Ca(PO_3)_2$:Eu^{3+} glass are presented. Chap.5 is devoted to the discussion of the laser-induced fluorescence spectrum. In Sec.5.1, the polarization characteristics of the fluorescence lines are analyzed, and the site symmetry of the Eu^{3+} ion in $Ca(PO_3)_2$ glass is determined and the fluorescence lines are assigned. Next, in Sec.5.2, from the analysis of the intensity of the $^5D_0$–$^7F_0$ fluorescence line, the transition mechanism of this line is attributed to the J-mixing effect. The energy dependence of the several levels on various local-field strengths is also analyzed. In Sec.5.3, the distribution of the site of the Eu^{3+} is discussed based on the analysis of the linewidth of the narrowed spectrum. Further, in Sec.5.4, the inhomogeneously broadened line shape of the $^5D_0$–$^7F_0$ line is discussed.

In Chap. 6, a conclusion of these investigations is presented.

2 Theory

2.1 Free ions of the Rare-Earth

The rare-earth ions are either divalent or trivalent in solids. Their electronic configurations are $4f^n5s^25p^6$ or $4f^{n-1}5s^25p^6$, respectively, where n is an integer. In our samples, the Eu ions are trivalent with the electronic configuration of $4f^65s^25p^6$. The $4f$ electrons are shielded from external field by two electronic shells of $5s^2$ and $5p^6$. Therefore, their spectra have atomic nature in character. Then, the consideration of the atomic energy levels is very important for the understanding of the optical spectra between the $4f$ levels of the rare-earth ion.

Generally, the electrons other than the $4f$ electrons contribute to the screening of the $4f$ electrons from the nucleus charge and the external field. However, these electrons do not contribute significantly to the relative separation of the $4f$ energy levels. Therefore, the explicit effect of these electrons can be neglected, and we consider the following Hamiltonian that determines the $4f^n$ energy levels of the rare-earth ion

$$\mathcal{H} = -\frac{\hbar^2}{2m}\sum_{i=1}^{n}\Delta_i - \sum_{i=1}^{n}\frac{Z^*e^2}{r_i} + \sum_{i<j}^{n}\frac{e^2}{r_{ij}} + \sum_{i=1}^{n}\zeta(r_i)\mathbf{s}_i\cdot\mathbf{l}_i\ , \qquad (2\text{-}1)$$

where Z^*e is the screened charge of the nucleus, and $\zeta(r_i)$ is the spin-orbit coupling coefficient. The first term in the Hamiltonian (2-1) is the kinetic energy of the $4f$ electrons and the second term is their Coulomb interaction with the nucleus. Since these terms of the Hamiltonian are spherically symmetric, the degeneracies of the energy levels within the $4f^n$ configuration are not removed by these interactions. Then, we neglect these terms in the following discussion.

The next two terms represent the mutual Coulomb interaction ($\mathcal{H}_C$) within the $4f$ electrons and their spin-orbit ($\mathcal{H}_{SO}$) interaction, respectively. We can consider the two limiting cases for the relative values of these two interactions; $\mathcal{H}_C \ll \mathcal{H}_{SO}$ and $\mathcal{H}_C \gg \mathcal{H}_{SO}$. For $\mathcal{H}_C \ll \mathcal{H}_{SO}$ we have the so-called j-j coupling

scheme, where the Coulomb interaction is treated as a small perturbation. On the other hand, the second limiting case is that the Coulomb interaction is large compared to the spin-orbit coupling and we have the so-called Russell-Saunders coupling scheme. In this scheme, we can treat the spin-orbit coupling as a small perturbation. In rare-earth ions, unfortunately, these two terms are in about equal strength, and we have the so-called intermediate coupling. The energies of the free ion levels are usually calculated using the Russell-Saunders coupling scheme as a first approximation, and then the spin-orbit interaction is taken into account.

The mutual Coulomb Hamiltonian is diagonal in the total orbital angular momenta L and total spin S. Then, a Russell-Saunders state is expressed as $|f^n\, \nu\, L\, S\, M_L\, M_S>$. Here, ν denotes the quantum number to distinguish between the same L-S states, and M_L, M_S are the projection of **L** and **S** on the z-axis, respectively. The energies of these states are obtained by the calculation of the mutual Coulomb terms. The first procedure of this calculation is that the two electron operator $1/r_{ij}$ in the mutual Coulomb term is developed in Legendre polynomial series. Then, we can separate the angular part from the radial part. The radial integral is so-called Slater integral which is usually denoted by $F_k(k = 2, 4, 6)$. The angular part is calculated by the tensor operator algebra which was chiefly developed by Racah [Ra 43, Ra 49]. This calculation is rather simple for the $4f^2$ states. However, the calculation is complicated for the $4f^6$ states of the Eu^{3+} ion. The solution of this electro-static interaction on the Eu^{3+} ion has been given by Gruber and Conway[GrCo 61].

Next, we consider the spin-orbit interaction. The Hamiltonian, which contains the spin-orbit interaction, is diagonal in the total angular momentum J. Then, L and S are no longer good quantum numbers. This interaction mixes the same J states of the Russell-Saunders states and removes the degeneracy of the J multiplets. We can also calculate $(\mathcal{H}_{SO})$ by separating the angular part from the radial part which is usually denoted by ζ_{4f}. The solution of the Eu^{3+} case has been given by Ofelt[Of 63]. His result indicates that the

Russell-Saunders states are rather good approximation for the ^7F states of the Eu^{3+} ion, though not for ^5D states.

The radial integrals are usually treated as free parameters which are adjusted to the experimentally observed energy levels, because the calculation of these integrals is very complicated.

In this thesis, we treat the wave function of the free Eu^{3+} ion as the intermediate coupling state which is expressed by the linear combination of Russell-Saunders states as follows:

$$|f^6[LS]J>=\sum_{L'S'}\alpha_J(^{2S+1}L;^{2S'+1}L')|f^6\,L'S'J> \quad . \tag{2-2}$$

Here [ ] shows that the quantities in the parentheses are not good quantum numbers. Further, the ^7F states are sometimes regarded as pure Russell-Saunders states because $\alpha_J(^7F;^7F)$ is known to be almost unity from the Ofelt's work [Of 63]. In the following sections, the crystal-filed splitting of the ^7F states will be calculated by regarding ^7F as pure Russell-Saunders states.

2.2 Parameterization of the Crystal Field

When the rare-earth ion is doped in some material, such as a crystal or a glassy matrix, it is exposed to the external field due to the charge of the ligands surrounding the rare-earth ion. This external field is the so-called crystal field or ligand field. Since the $4f$ electrons are shielded by the outer electronic shells ($5s$ and $5p$), the effect is usually very small compared with the mutual Coulomb interaction and the spin-orbit interaction. Therefore, we can usually regard the crystal-field interaction as a perturbation. This is quite different from the case of the electronic states of the transition metal ions, where the d electrons are strongly affected by the crystal-field interaction. If we take into account this interaction, partial removing of the degeneracy of the $^{2S+1}L_J$ manifolds and also mixing of states belonging to the same irreducible representation may occur.

Let us expand the crystal-field potential acting on a rare-earth ion as

$$\mathrm{V}_c = \sum_{kq} \sum_{j} B_{kq} C_q^{(k)}(\theta_j, \phi_j) \ , \tag{2-3}$$

with

$$C_q^{(k)}(\theta_j, \phi_j) = \sqrt{\frac{4\pi}{(2k+1)}}\, Y_q^{(k)}(\theta_j, \phi_j) \ ,$$

where $Y_q^{(k)}(\theta_j, \phi_j)$ is the q-component of k-th order spherical harmonics and (r_j, θ_j, ϕ_j) is the position of the j-th $4f$ electron of the rare-earth ion. B_{kp} is a q-component of k-th order crystal-field parameter. Here, if the crystal has a charge density $\rho(\mathrm{R})$, the crystal-field potential is expressed by the space integral with respect to the position R as

$$\begin{aligned} \mathrm{V}_c &= -\sum_j \int \frac{e\rho(\mathrm{R})}{|\mathrm{R} - \mathrm{r}_j|} d\tau \\ &= -\sum_{k,j} e \int \rho(\mathrm{R}) P_k(\cos(\mathrm{R}, \mathrm{r}_j)) \frac{r_<^k}{r_>^{k+1}} d\tau \ , \end{aligned} \tag{2-4}$$

where r_j is the coordinate of the j-th electron, and $r_<$ and $r_>$ denote the smaller and larger values of $|\mathrm{R}|$ and $|\mathrm{r}_j|$, respectively. P_k is the k-th order of the Legendre polynomial and $(\mathrm{R}, \mathrm{r}_j)$ is the angle between R and r_j. Since the Legendre polynomial is expressed by the product of the two spherical harmonics, we obtain

$$\begin{aligned} \mathrm{V}_c &= -\sum_{k,q} \sum_j e \int \rho(\mathrm{R}) \frac{4\pi}{2k+1} (-)^q Y_q^{(k)}(\theta_j, \phi_j) Y_{-q}^{(k)}(\theta, \phi) \frac{r_<^k}{r_>^{k+1}} d\tau \\ &= -\sum_{k,q} \sum_j e \int (-)^q \rho(\mathrm{R}) C_q^{(k)}(\theta_j, \phi_j) C_{-q}^{(k)}(\theta, \phi) \frac{r_<^k}{r_>^{k+1}} d\tau \\ &= \sum_{k,q} \sum_j B_{kq} C_q^{(k)}(\theta_j, \phi_j) \ , \end{aligned}$$

where B_{kq} is defined by

$$B_{kq} \equiv -e \int (-)^q \rho(\mathrm{R}) C_{-q}^{(k)}(\theta, \phi) \frac{r_<^k}{r_>^{k+1}} d\tau \ . \tag{2-5}$$

Here, since B_{kq} includes all radial components of the crystal-field potential, we can calculate the crystal-field matrix elements except B_{kq}. The matrix element of the crystal-field potential between the two Russell-Saunders states is obtained by the tensor operator technique as

$$< f^N\, S\, L\, J\, M_J |\, \mathrm{V}_c\, | f^N\, S\, L'\, J'\, M'_J > = \sum_{kq} B_{kq} < f^N\, S\, L\, J\, M_J |\, U_q^{(k)} | f^N\, S\, L'\, J'\, M'_J >< f \,\|\, C^{(k)} \,\|\, f > , \tag{2-6}$$

$$< f^N\, S\, L\, J\, M_J |\, U_q^{(k)} | f^N\, S\, L'\, J'\, M'_J > = (-)^{J-M_J} \begin{pmatrix} J & k & J' \\ -M_J & q & M'_J \end{pmatrix} < f^N\, S\, L\, J \,\|\, U^{(k)} \,\|\, f^N\, S\, L'\, J' > , \tag{2-7}$$

and

$$< f^N\, S\, L\, J \,\|\, U^{(k)} \,\|\, f^N\, S\, L'\, J' > = (-)^{S+L'+J+k} [(2J+1)(2J'+1)]^{1/2} \times \begin{Bmatrix} J & J' & k \\ L' & L & S \end{Bmatrix} < f^N\, S\, L \,\|\, U^{(k)} \,\|\, f^N\, S\, L' > , \tag{2-8}$$

where $U^{(k)}$ is a k-th order unit tensor operator, and $< \cdots \| U^{(k)} \| \cdots >$ denotes a reduced matrix element of $U^{(k)}$. The 3-j symbols and 6-j symbols are calculated by the formula of Racah, and the reduced matrix elements for the f states have been tabulated by Nielson and Koster[NiKo 64]. The calculation of B_{kq} which contains the radial integral of the matrix element is almost impossible. Therefore, we treat B_{kq} as a parameter determined by experimental data. In the intermediate coupling scheme, the wave functions are usually given as a linear combination of the Russell-Saunders basis set functions. Therefore, the energies of Stark levels of their multiples are evaluated as a linear combination of the matrix elements between the pure Russell-Saunders states. However, usually, the calculation of these energies is rather complicated.

The energies and wave functions of the rare-earth ion under the crystal-field potential are expressed using Eqs.(2-6)–(2-8). Usually, the perturbation calculation is made for the zeroth-order and the first-order which give the so-called Stark splitting and J-mixing of the manifolds, respectively. The higher order terms of this perturbation calculation are usually small, so that these terms are usually neglected.

2.3 Calculation of the ^7F levels of the Eu^{3+}

In this section, we calculate the energies of the Stark levels of the $^7F_1$ manifold and the $^7F_0$ level of the Eu^{3+} ion. Because $\alpha_J(^7F\,;^7F)$ is almost unity, we regard the ^7F states of a free Eu^{3+} ion as pure Russell-Saunders states. As discussed later, the point symmetry of the Eu site in $Ca(PO_3)_2$ is readily shown to be restricted to C_S, C_2, C_{2V} and D_2. Since $B_{2\pm1}$ are absent in these point symmetries, hereafter we put $B_{2\pm1} = 0$. If the crystal-field mixing of states other than $^7F_1$ is neglected, only the second-order term $V_c^{(2)}$ of Eq.(2-3) contributes to the crystal-field splitting of $^7F_1$ and the eigen functions and the energies of the three components are calculated as

$$\Psi_1 = |0>\,, \tag{2-9}$$

$$\Psi_2 = (\theta\,|+1> - |-1>)/\sqrt{2}\,, \tag{2-10}$$

$$\Psi_3 = (\theta\,|+1> + |-1>)/\sqrt{2}\,, \tag{2-11}$$

and

$$E(\varepsilon_1) = E_0(^7F_1) + X/5\,, \tag{2-12}$$

$$E(\varepsilon_2) = E_0(^7F_1) - X/10 - \sqrt{6}Y/10\,, \tag{2-13}$$

$$E(\varepsilon_3) = E_0(^7F_1) - X/10 + \sqrt{6}Y/10\,, \tag{2-14}$$

where $\theta = B_{22}/|B_{22}|$, $X \equiv B_{20}$, $Y \equiv |B_{22}| = |B_{2-2}|$, and $E_0(^7F_1)$ is the energy of the $^7F_1$ state in the case of $V_c^{(2)} = 0$. Further, if we take into account the mixing of other states through $V_c^{(2)}$, using the first order perturbation calculation, we obtain

$$E(\varepsilon_1) = E_0(^7F_1) + X/5 - 9\beta X^2 - 2(5\beta + 4\gamma)Y^2\,, \tag{2-15}$$

$$E(\varepsilon_2) = E_0(^7F_1) - X/10 - \sqrt{6}Y/10 - 3(2\beta + \gamma)X^2 - 2(8\beta + \gamma)Y^2 - 2\sqrt{6}(\beta - \gamma)XY\,, \tag{2-16}$$

$$E(\varepsilon_3) = E_0(^7F_1) - X/10 + \sqrt{6}Y/10 - 3(2\beta + \gamma)X^2 - 2(8\beta + \gamma)Y^2 + 2\sqrt{6}(\beta - \gamma)XY\,, \tag{2-17}$$

where $\beta = 2/525\Delta_{31}$, $\gamma = 1/300\Delta_{21}$ and $\Delta_{JJ'}$ is the energy separation between ^7F_J and $^7F_{J'}$ at $V_c = 0$. Similarly, if we consider only the effect of $V_c^{(2)}$, the energy of the $^7F_0$ state is expressed, using $\alpha = 4/75\Delta_{20}$, as

$$E(^7F_0) = E_0(^7F_0) - \alpha(X^2 + 2Y^2) . \tag{2-18}$$

In a later section, we analyze our experimental data using these expressions and the following notation as $E_{JJ'} = E(^7F_{J'}) - E(^5D_J)$.

2.4 Optical Transition Probability of the Eu^{3+} ion

In this section, we calculate the transition probability of the $^5D_0$–$^7F_0$ transition of the Eu^{3+} ion.

In general, the electric dipole transition between the $4f$ states is forbidden. However, if the odd term of the external-field potential acts on the rare-earth ions, the different parity states mix into the $4f$ states. Therefore, the electric dipole transition can be partially allowed. This transition probability has been calculated by Judd and Ofelt [Ju 62, Of 62]. However, in this theory the $^5D_0$–$^7F_0$ transition is not allowed. Further, the $^5D_0$–$^7F_0$ transition due to the magnetic dipole and electric quadrupole is also forbidden. Two probable mechanisms of the $^5D_0$–$^7F_0$ transition are suggested. One is the mixing of the odd parity states, which are not considered in the Judd-Ofelt theory, due to the odd term of the crystal-field potential, and the other is borrowing the intensity from the $^5D_0$–$^7F_2$ transition due to the mixing of the even term of the crystal-field potential[Wy 67].

First, we consider the mixing of odd-parity states. If we consider only the odd-parity crystal-field potential V_c^{odd}, the first-order perturbation calculation gives the wave function for the $^7F_0$ state as

$$|[f^6\,^7F_0]> = |f^6[^7F]_0> + \sum_{A_J} |A_J> \frac{<A_J|\,V_c^{odd}\,|f^6[^7F]_0>}{E_0(f^6[^7F]_0) - E_0(A_J)} , \tag{2-19}$$

where $E_0(\ )$ is the energy of the state in the parentheses, and A_J includes odd-parity charge transfer states (CTS) as well as $4f^5 5d$ and $4f^5 5g$ configurations. The wave function for the $^5D_0$ state is obtained by replacing ^7F by ^5D. Then, since $< [f^6\,{}^5D]_0 |\, \mathbf{P} \,| [f^6\,{}^7F]_0 >$ is zero, the matrix element of the electric dipole moment $\mathbf{P}$ between the $^5D_0$ and $^7F_0$ states is given by

$$< [f^6\,{}^5D_0] || \, \mathbf{P} \, | [f^6\,{}^7F_0] > =$$

$$\sum_{A_J} \left(\frac{< f^6\,[^5D]_0 |\, \mathbf{V}_c^{odd} \,| A_J >< A_J |\, \mathbf{P} \,| f^6\,[^7F]_0 >}{E_0(f^6\,[^5D]_0) - E_0(A_J)} \right.$$

$$\left. + \frac{< f^6\,[^5D]_0 |\, \mathbf{P} \,| A_J >< A_J |\, \mathbf{V}_c^{odd} \,| f^6\,[^7F]_0 >}{E_0(f^6\,[^7F]_0) - E_0(A_J)} \right) . \qquad (2\text{-}20)$$

Since $\alpha_0(^7F\,;{}^7F)$ is almost unity[Of 63], Eq.(2-20) is approximated by multiplying the right-hand side by $\alpha_0(^5D\,;{}^7F)\alpha_0(^7F\,;{}^7F)$ and replacing $[^5D]_0$ and $[^7F]_0$ in the numerators by $^7F_0$. Therefore, the electric dipole $^5D_0$–$^7F_0$ transition is partially allowed by the mixing of the septet state with $J = 1$ through the linear term of the local-field potential $\mathbf{V}_c^{(1)}$. This mechanism is consistent with the well-known fact that the rather intense $^5D_0$–$^7F_0$ transition is observed only when the crystal-field potential includes a linear term[NiBl 66, NiBl 67]. In the Judd-Ofelt theory, which employs the closure approximation, all the energy denominators in Eq.(2-20) are assumed to be the same. Then, $< [f^6\,{}^5D_0] || \, \mathbf{P} \, | [f^6\,{}^7F_0] >$ becomes proportional to $< f^6\,{}^5D \,||\, U^{(0)} \,||\, f^6\,{}^7F >$. This reduced matrix element of the unit tensor operator $U^{(0)}$ is zero because of the orthogonality of the two wave functions. Hence, the $^5D_0$–$^7F_0$ transition is not permitted by the Judd-Ofelt theory. On the other hand, this theory explains the $^5D_0$–^7F_J $(J = 2, 4, 6)$ and ^5D_J–$^7F_0 (J = 2, 4)$ transitions well. The matrix element of $\mathbf{P}$ is written in these cases using the reduced matrix elements of $U^{(\lambda)}$ with $\lambda = 2, 4$ and 6, which are usually nonzero.

When only some high-lying odd-parity states make a dominant contribution, the closure approximation does not apply well, and the matrix element of Eq.(2-20) is not necessarily very small. The CTS, whose energy lies lower than

that of the $4f^5 5d$ and $4f^5 5g$ configurations in the case of Eu^{3+}[JoPa 64], may be the most probable high-lying state of this kind[HoIm 77]. For Eu^{3+}, the CTS is considered to be split largely into two in energy and the lower states are only septet and nonet[HoIm 77]. It is possible that this septet admixes into $^7F_0$ through $V_c^{(1)}$ and allows the forbidden $^5D_0$–$^7F_0$ transition.

Next, we consider the mixing due to the even-parity crystal-field potential V_c^{even}. In this case, in a similar way as Eq.(2-19), the wave function for the $^7F_0$ state can be written as

$$|f^6\,[^7F_0]> = |f^6\,[^7F]_0> + \sum_{J\neq 0} |f^6\,[^7F]_J> \frac{<f^6\,[^7F]_J|\,V_c^{even}\,|f^6\,[^7F]_0>}{E_0(f^6\,[^7F]_0) - E_0(f^6\,[^7F]_J)} . \tag{2-21}$$

Here, we have considered only the mixing of nearby ^7F_J states for which the energy denominators are small. The wave function for the $^5D_0$ state is obtained by replacing ^7F by ^5D. Since the electric dipole transition within $4f$ configuration is allowed due to the odd-term of the crystal-field potential, the wave function concerned for the $^5D_0$–$^7F_0$ transition is obtained similarly as

$$|[f^6\,{}^7F_0]) = |f^6\,[^7F_0]> + \sum_{A_J} |A_J> \frac{<A_J|\,V_c^{odd}\,|f^6\,[^7F_0]>}{E_0(f^6\,[^7F_0]) - E_0(A_J)} . \tag{2-22}$$

Here, the wave function in which the J-mixing is taken account is denoted by $|\ )$. Even if the order of the J-mixing effect due to V_c^{even} and the mixing of the high-lying states due to V_c^{odd} changes for the perturbation calculation, the final expression as Eq.(2-22) does not change under the second-order crystal-field mixing. Therefore, we calculate the transition probability with this wave function. Here, in this calculation, we neglect the mixing terms higher than second order. Then, we obtain the matrix element of the electric dipole moment P between the $^7F_0$ and $^5D_0$ states as

$$([f^6\,{}^5D_0]|\,\mathrm{P}\,|[f^6\,{}^7F_0]) = <[f^6\,{}^5D_0]|\,\mathrm{P}\,|[f^6\,{}^7F_0]> + \sum_{\mathrm{J}\neq 0} \left(\frac{<f^6\,[^7F]_{\mathrm{J}}|\,V_c^{even}\,|f^6\,[^7F]_0>}{E_0(f^6\,[^7F]_0) - E_0(f^6\,[^7F]_J)} <[f^6\,{}^5D_0]|\,\mathrm{P}\,|[f^6\,{}^7F_{\mathrm{J}}]> \right.$$

$$+\frac{<f^6\,[^5D]_0|\,\mathrm{V}_c^{even}\,|f^6\,[^5D\,]_\mathbf{J}>}{E_0(f^6\,[^5D]_0)\,-\,E_0(f^6\,[^5D\,]_J)}<[f^6\,{}^5D_\mathbf{J}]|\,\mathbf{P}\,|[f^6\,{}^7F_0]>\Bigg)\ ,$$

(2-23)

and

$$<[f^6\,{}^5D_{\mathbf{J}'}]|\,\mathbf{P}\,|[f^6\,{}^7F_\mathbf{J}]>=$$

$$\sum_{A_J}\Bigg(\frac{<f^6\,[^5D]_{\mathbf{J}'}|\,\mathrm{V}_c^{odd}\,|A_J><A_J|\,\mathbf{P}\,|f^6\,[^7F]_\mathbf{J}>}{E_0(f^6\,[^5D]_{J'})\,-\,E_0(A_J)}$$

$$+\frac{<f^6\,[^5D]_{\mathbf{J}'}|\,\mathbf{P}\,|A_J><A_J|\,\mathrm{V}_c^{odd}\,|f^6\,[^7F]_\mathbf{J}>}{E_0(f^6\,[^7F]_J)\,-\,E_0(A_J)}\Bigg)\ , \qquad (2\text{-}24)$$

where J denotes the set of the quantum numbers J, M_J. The first term in the right-hand side of Eq.(2-23) is similar to the matrix element of Eq.(2-20). The second summation is the J-mixing term, and each term in the brackets indicates the intensity borrowed from $^5D_0$–^7F_J and ^5D_J–$^7F_0$ transitions, respectively. Further, the matrix elements of P of the right hand side of these terms, which are expressed as Eq.(2-24), can be evaluated, for the case of $^5D_0$-^7F_J $(J = 2, 4, 6)$ and ^5D_J–$^7F_0$ $(J = 2, 4)$, by Judd-Ofelt theory, as mentioned above. Thus, the electric dipole $^5D_0$–$^7F_0$ transition is partially allowed by the mixing of ^7F_J $(J = 2, 4, 6)$ and ^5D_J $(J = 2, 4)$ multiplets into the $^7F_0$ and $^5D_0$ states, respectively. Especially, the mixing of $^7F_2$ into $^7F_0$ by the second-order terms of the crystal-field potential will play the dominant role, because the energy denominator is much smaller than the cases of $^7F_{4,6}$ and $^5D_{2,4}$ states and also because the fluorescence intensity of the $^5D_0$–$^7F_2$ transition is much higher than those of the $^5D_0$–$^7F_{4,6}$ transitions.

3 Experimental Procedure

3.1 Glass Samples

Three $Ca(PO_3)_2$:Eu^{3+} glass samples which were kindly supplied by Professor E.Takushi of University of the Ryukyus were used in our experiment. These samples were prepared by dehydrating the mixture of $Ca(H_2PO_3)_2 \cdot H_2O$, Eu_2O_3 and H_3PO_4 in aluminum crucible for 12 hours and heating it at 1200 $\sim$ 1300°C for 30 $\sim$ 40 minutes. Then, the crucible was taken out from the furnace and the fusion was poured and cooled to room temperature. Thus, a glass of about 1.0 cm in diameter and about 5 mm in thickness which was colored pink was obtained. The samples of 3 mm in thickness and 10 mm in diameter were used after polishing the three faces with alumina powder. Three glass samples contain 1.4, 12 and 24 mol% of Eu_2O_3. The spectral properties of these samples did not change during this experiment (about five years). However, these samples are rather fragile. When the sample was soaked rapidly in liquid N_2 or pulled up, the sample sometimes cracked. However, there was no difference in the fluorescence properties between the cracked sample and the not cracked sample.

3.2 Experimental Setup

The excitation source for the $^7F_0$–$^5D_1$ and $^7F_1$–$^5D_1$ absorption lines was a cw coumarin 535 dye laser pumped by the 488.0 nm line of an Ar^+ ion laser (Spectra Physics model 164). A Lyot filter was inserted in the dye laser cavity and the laser light was tunable in the 523 $\sim$ 537 nm wavelength range with a spectral width (half width at half maximum; HWHM) of about 1 cm^{-1}. A rhodamine 6G dye laser was also used for the $^7F_0$–$^5D_0$ and $^7F_1$–$^5D_0$ excitations. By passing the laser beam through a monochromator (Nikon model G250), the broad emission from the dye laser was rejected before the excitation of

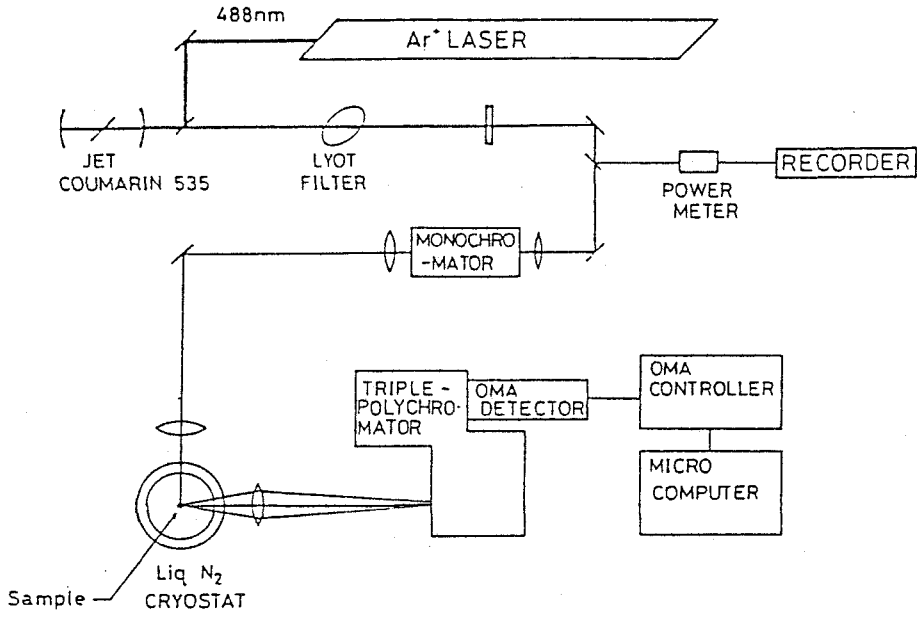

Figure 3.1: Typical experimental setup.

the sample. The sample temperature was maintained at 77K in the liquid N_2 cryostat. The emission spectrum was measured with a triple-grating polychromator (Spex model 1877) and an intensified Si-photodiode-array detector (Princeton Applied Research model 1420) cooled at about $-20°C$. The dark signals were subtracted from the accumulated data using a microcomputer. The wavelength axis of the Si-photodiode-array detector was calibrated by Ne and Na fluorescence lines emitted by a hollow cathode lamp (Hamamatsu L733–201NB). The double monochromator (Spex model 14018) equipped with a cooled photomultiplier (Hamamatsu R–928) was also used in our measurements. In this case, the spectra were detected by the photon counting method. The parts of the spectral data were smoothed using a microcomputer. An deuterium lamp (ORIGINAL HANAU model D200F) with a UV bandpass filter (Toshiba UVD33S) was used for the broad band excitation in the UV region. The typical experimental setup is shown in Fig.3.1.

4 Experimental Results

4.1 The Narrowed Fluorescence Spectra

The fluorescence spectra of the sample were measured for various excitation energies within the $^7F_0$,$^7F_1$–$^5D_0$,$^5D_1$ absorption bands. The results were almost the same for samples with different Eu concentrations except for the emission intensity. Therefore, the measurements were made on the sample with 23.5mol% of Eu_2O_3 which showed most intense emission from the $^5D_0$ state. Fig.4.1 shows the emission spectrum of the $^5D_0$–$^7F_0$,$^7F_1$,$^7F_2$ bands at 77K under the ultra-violet light excitation by a deuterium lamp with a UVD–33S filter to cut the visible light. The most intense emission of this glass is the $^5D_0$–$^7F_2$ line. The spectrum of the $^5D_0$–$^7F_0$ line is asymmetric with a longer tail in the high-energy side. The $^5D_0$–$^7F_1$ emission is split into three lines. These spectra are almost independent of temperature. The emissions originating from the $^5D_1$ states are very weak. Indeed, the intensity of the $^5D_1$–$^7F_1$ emission is about 1% of that of the $^5D_0$–$^7F_1$ emission under the 476.5nm excitation.

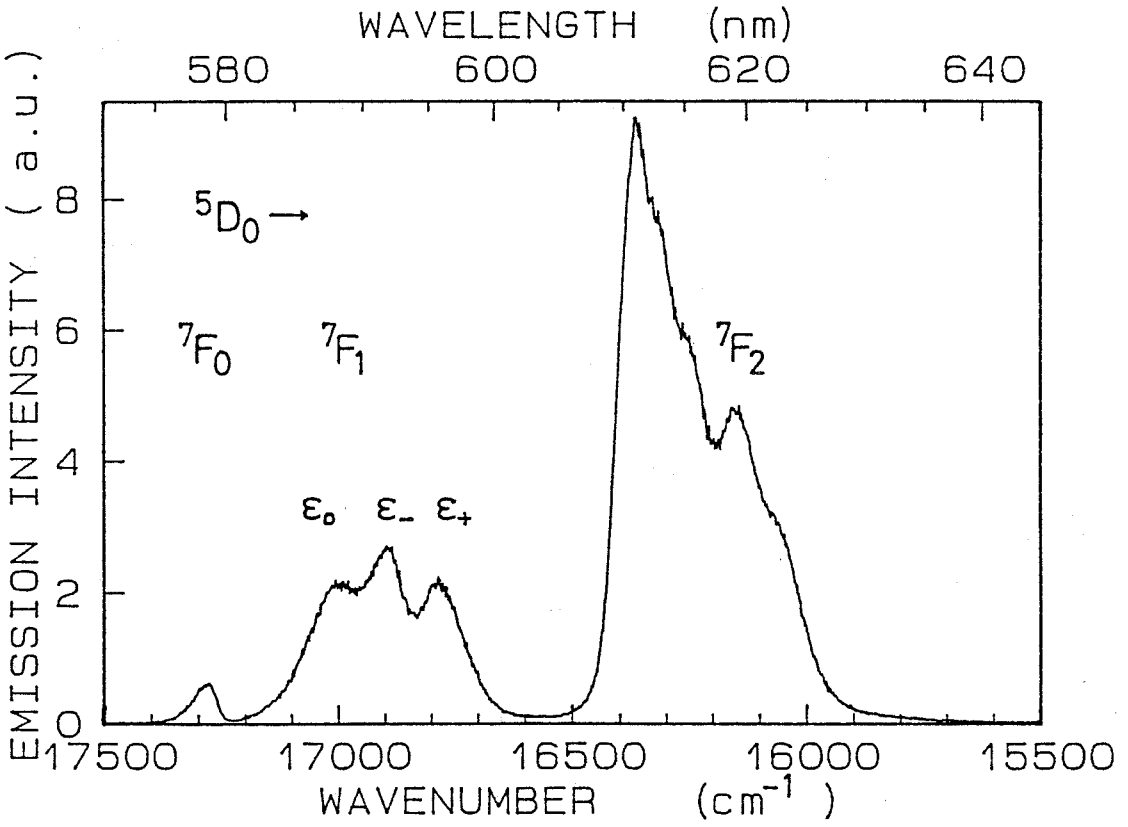

Figure 4.1: Fluorescence spectrum of Eu^{3+} in $Ca(PO_3)_2$ glass at 77K with excitation of the broad ultraviolet band by a deuterium lamp.

Figs.4.2 (a) through (d) show the emission spectra due to the $^5D_0$–$^7F_0$, $^7F_1$ transitions at 77K for various excitation energies within the $^7F_0$, $^7F_1$–$^5D_0$, $^5D_1$ absorption bands. Intensities are normalized to the most intense $^5D_0$–$^7F_1$ peak. We name the Stark levels of the $^7F_1$ and $^5D_1$ manifolds as ε_+ , ε_- , ε_0 and δ_+ , δ_- , δ_0 in order of decreasing energy, respectively(cf. Fig.4.4). The line-narrowing effect is observed for the $^5D_0$–$^7F_0$ and $^5D_0$–ε_0 lines, but is not clear for the $^5D_0$–$\varepsilon_\pm$ lines which are rather broad. Both the $^5D_0$–$^7F_0$ and $^5D_0$–ε_0 lines move toward lower energies with decreasing excitation energy. On the other hand, the positions of the $^5D_0$–$\varepsilon_\pm$ lines are almost insensitive to the excitation energy. However, we have observed the small shift of these lines for excitations in the low-energy side of the absorption bands. The energies of emission lines change continuously and we have not observed the lines to disappear or new lines to appear unexpectedly. Therefore, the crystal-field strength acting on the Eu^{3+} ion is considered to change continuously in this material.

Figure 4.2: (next page) Narrowed fluorescence spectra of Eu^{3+} in $Ca(PO_3)_2$ glass at 77K in the spectral region of the $^5D_0$–$^7F_0$ and $^5D_0$–$^7F_1$ transitions for various excitation wavenumbers in the $^7F_0$–$^5D_0$: (a), $^7F_1(\varepsilon_0)$–$^5D_0$: (b), $^7F_0$–$^5D_1$: (c) and $^7F_1(\varepsilon_0)$–$^5D_1$: (d) absorption bands.

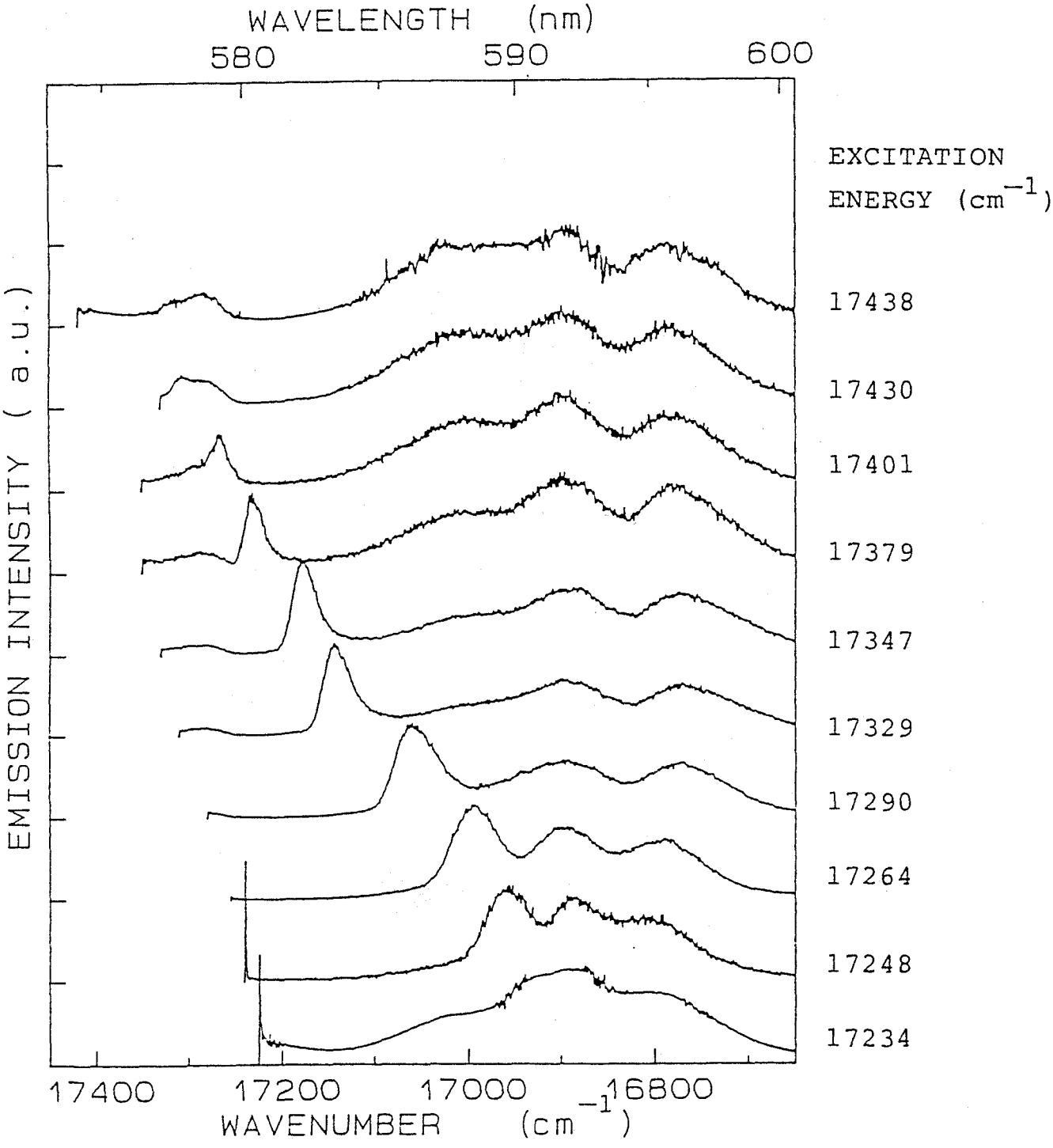

Figure 4.2: (a) The $^7F_0$–$^5D_0$ excitation

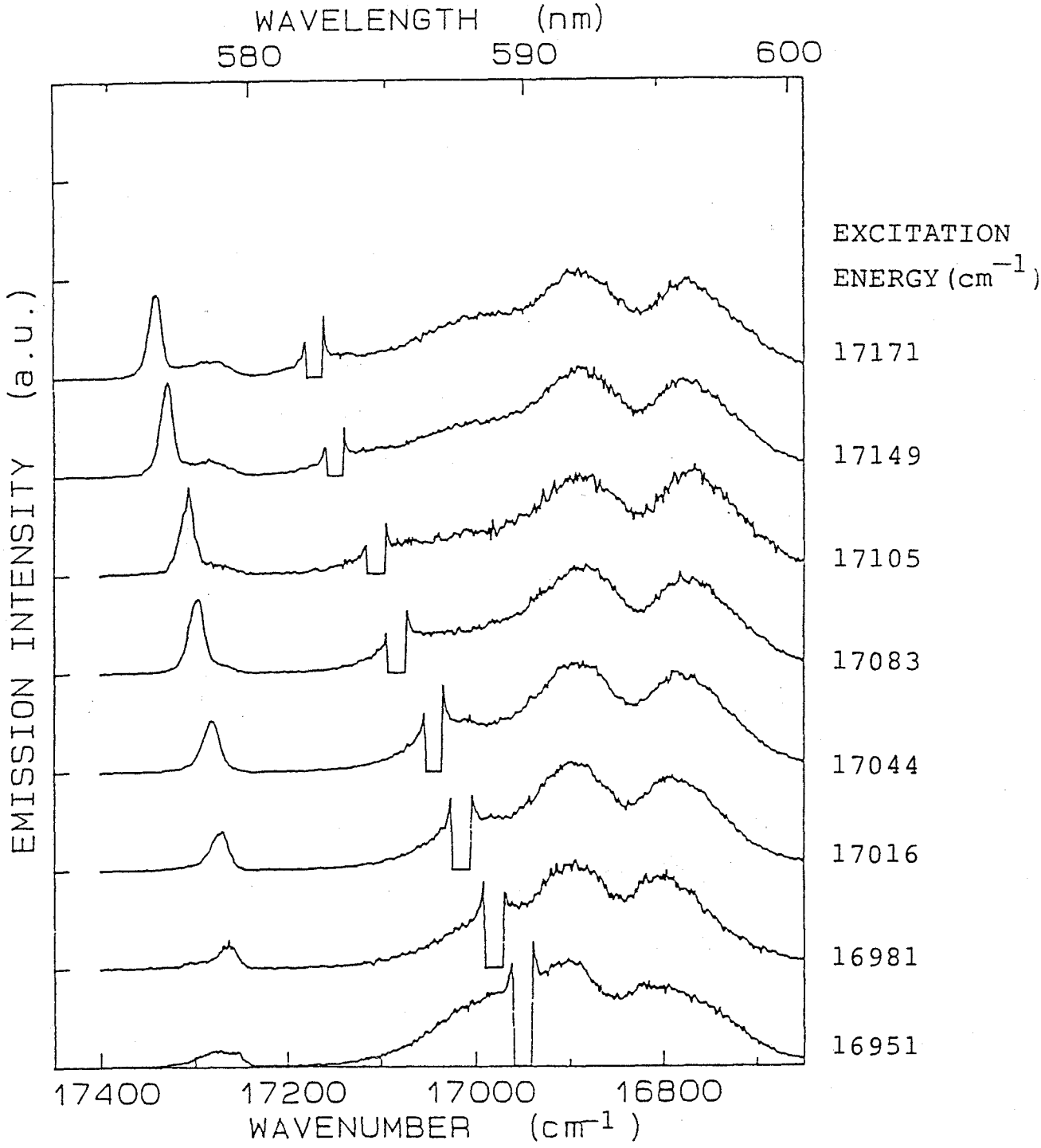

Figure 4.2: (b) The $^7F_1(\varepsilon_0)$–$^5D_0$ excitation

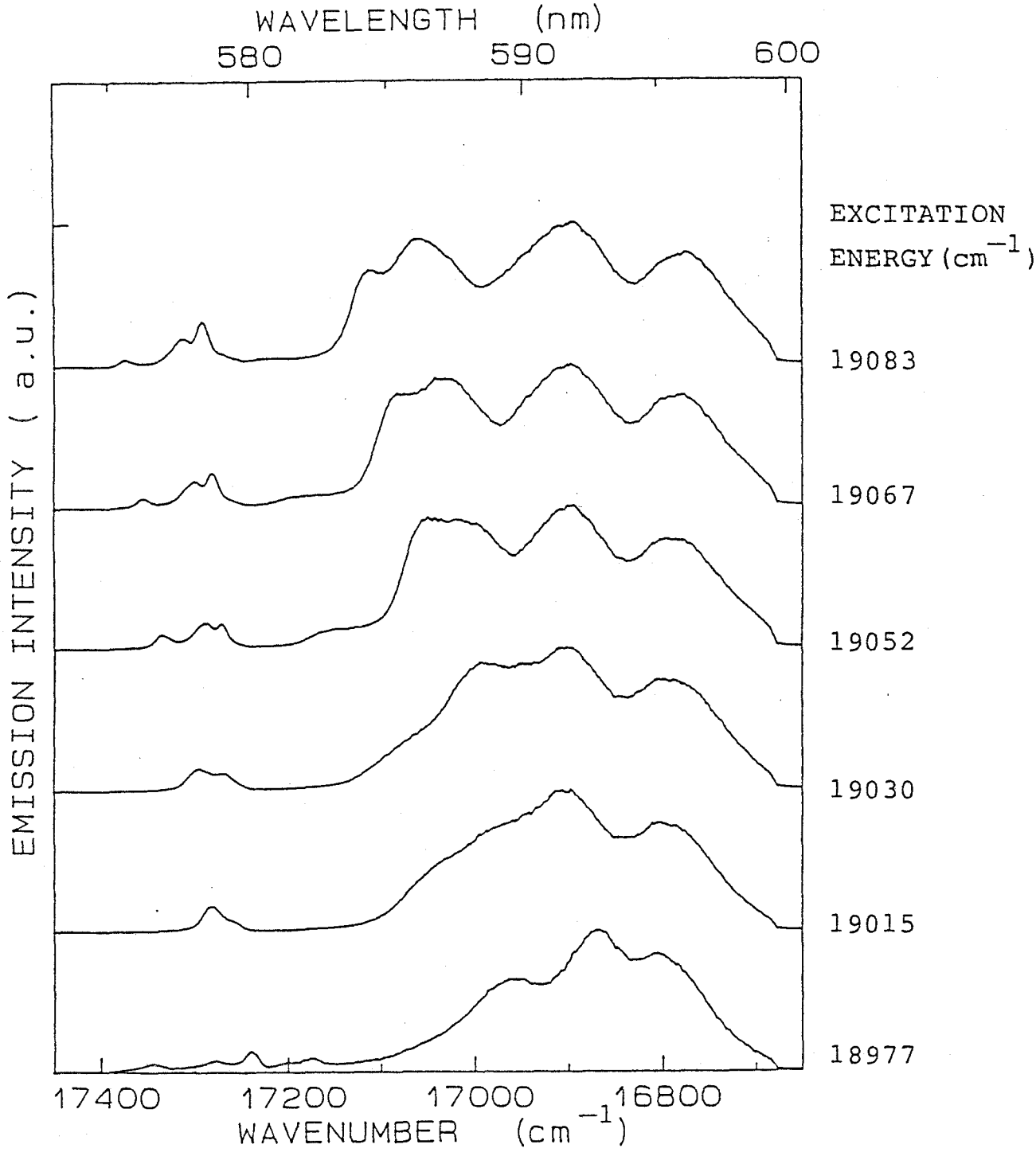

Figure 4.2: (c) The $^7F_0$–$^5D_1$ excitation

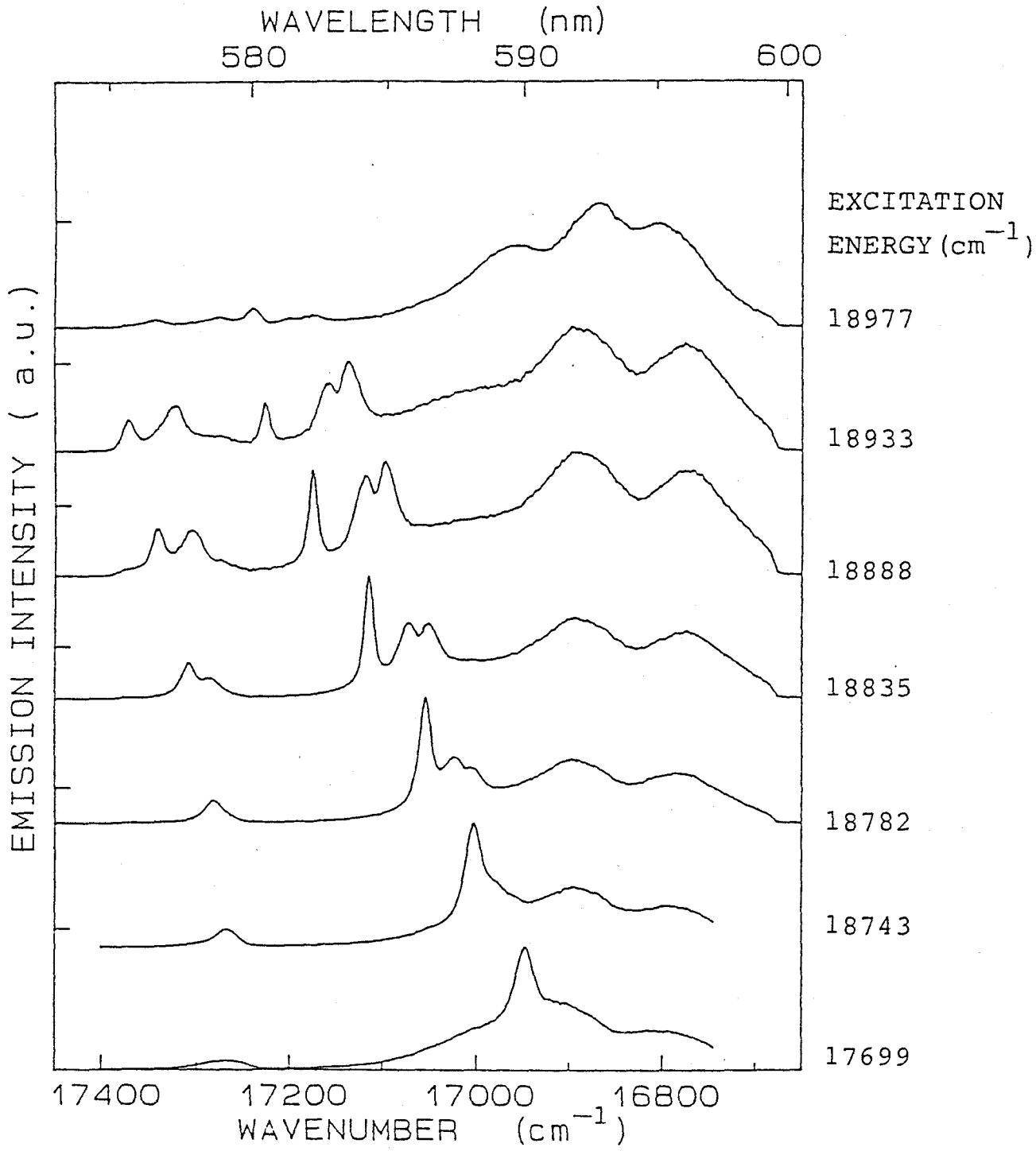

Figure 4.2: (d) The $^7F_1(\varepsilon_0)$–$^5D_1$ excitation

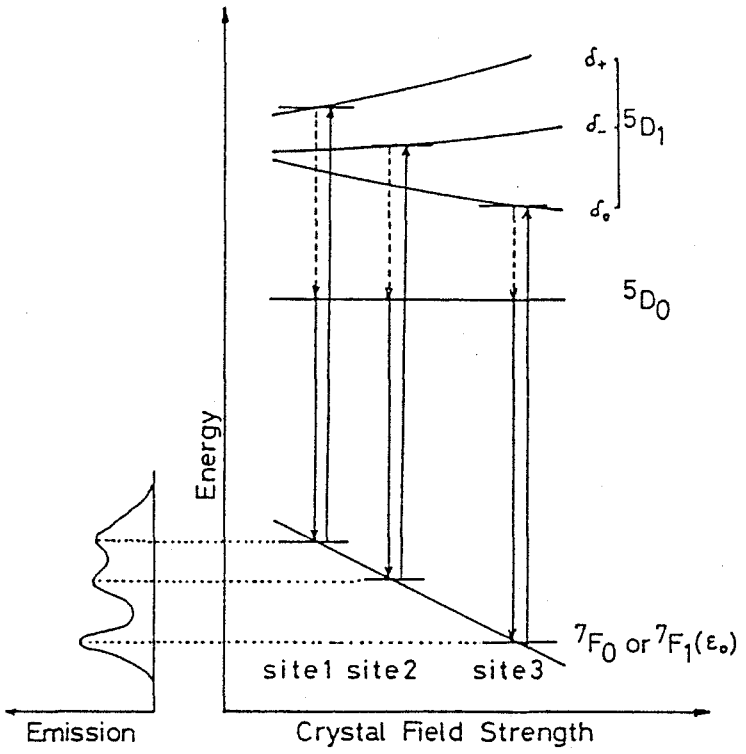

Figure 4.3: The energy-level scheme of Eu^{3+} in a glass. The vertical solid lines denote radiative transition, and dashed lines denote non-radiative transition. Ions in the site 1, site 2 and site 3 are in resonance with the excitation energy via different $^5D_1$ Stark levels.

Figs.4.2 (a) and (b) show the emission spectrum for the excitation within the $^7F_0, \varepsilon_0$–$^5D_0$ bands. The splitting energy between the $^5D_0$–ε_- and the $^5D_0$–ε_+ lines decreases with decreasing excitation energy when the excitation is made within the low-energy side of the absorption band. This effect is larger for excitation in the $^7F_0$–$^5D_0$ band than in the ε_0–$^5D_0$ band. A broad hump was observed at about 17000cm^{-1}around the $^5D_0$–ε_0 line, when the high-energy side of the absorption bands was excited. This broad hump is almost insensitive to the excitation energy, and is attributed to the energy transfer effect between the site in resonance and the other sites. We have observed a sideband beside the $^5D_0$–$^7F_0$ line, which is also attributed to the same effect. We have also observed these humps for excitation within the $^7F_1$–$^5D_1$ band, as shown in Figs.4.2 (c) and (d).

For excitation within $^7F_0$,$^7F_1$–$^5D_1$ absorption bands, as in Figs.4.2 (c) and (d), three narrow lines are observed, at maximum, in the spectral regions of the $^5D_0$–ε_0 and $^5D_0$–$^7F_0$ transitions. These three lines, which are attributed to the three Stark levels of the $^5D_1$ state are explained as follows. The inhomogeneous broadenings of the ε_0–$^5D_1$ and $^7F_0$–$^5D_1$ absorption lines are larger than the crystal-field splitting of the $^5D_1$ manifold in this glass. Therefore, for a given laser energy, three Eu^{3+} ions in different environment are excited, for which the energy separations between $^7F_0$ (or ε_0) level and the three Stark levels of $^5D_1$ are in resonance with laser. Because the $^5D_0$–ε_0 and $^5D_0$–$^7F_0$ energy separations are different for these ions, we observe three fluorescence lines. The three lines move toward lower energies with decreasing excitation energy. Therefore, the energy separation between the $^7F_0$ (or ε_0) state and the center of gravity of $^5D_1$ state decreases with decreasing energy between the $^7F_0$ (or ε_0) and $^5D_0$ states. Fig.4.3 shows the case that the three ions in different sites are selected with the excitation within the $^7F_0$–$^5D_1$ absorption bands[HeYe 78].

The number of the narrow lines decreases when the excitation energy is decreased, because the number of Stark levels of $^5D_1$ that can be reached in resonance decreases. On the other hand, the $^5D_0$–$^7F_0$ fluorescence spectrum splits only into two lines under the ε_0–$^5D_1$ excitation. We consider that the two low-energy fluorescence lines overlap with each other. With decreasing excitation energy, the two low-energy $^5D_0$–ε_0 lines become overlapped and the $^5D_0$–$^7F_0$ line structure becomes indistinct in Fig.4.2 (d). At very low excitation energies, the $^5D_0$–$^7F_0$ fluorescence line is rather broad, and the $^5D_0$–ε_0 line overlaps with the $^5D_0$–ε_- line.

4.2 The Energy Level Scheme

We have determined the energy separations between various levels of Eu^{3+} from the peak positions of emission lines under monochromatic light excitation of various excitation energies. As discussed later, the energy of the $^5D_0$ state is considered to be rather insensitive to the variation in the crystal field strength. Therefore, we have taken the energies of levels of the Eu^{3+} ion relative to the $^5D_0$ state. We plot the energies of several levels of the Eu^{3+} ion in Fig.4.4 as a function of the energy of the site-selected $^5D_0$–$^7F_0$ line. The results are shown by closed circles for the $^7F_0$–$^5D_0$ excitation, by closed triangles for the ε_0–$^5D_0$ excitation, by open circles for the $^7F_0$–$^5D_1$ excitation, and by open triangles for the ε_0–$^5D_1$ excitation. The energies of the levels determined by the excitation within various transitions almost agree with each other. However, the energies determined from measurement under the excitations of ε_0–$^5D_0$ and $^7F_0$–$^5D_0$ are different from each other. Particularly, when the $^7F_0$–$^5D_0$ energy decreases, there is a clear difference between these results. In Fig.4.4, we notice that there is a similarity in the splitting pattern between the $^5D_1$ and $^7F_1$ states. On the other hand, the quadratic relation between the energy of the $^5D_0$–$^7F_0$ line and that of the $^5D_0$-ε_0 line has been found. Further, the energy of the center of gravity of the three Stark levels of the $^7F_1$ manifold has been found to be linearly correlated with the energy of the $^5D_0$–$^7F_0$ line, as shown by a solid line in Fig.4.5.

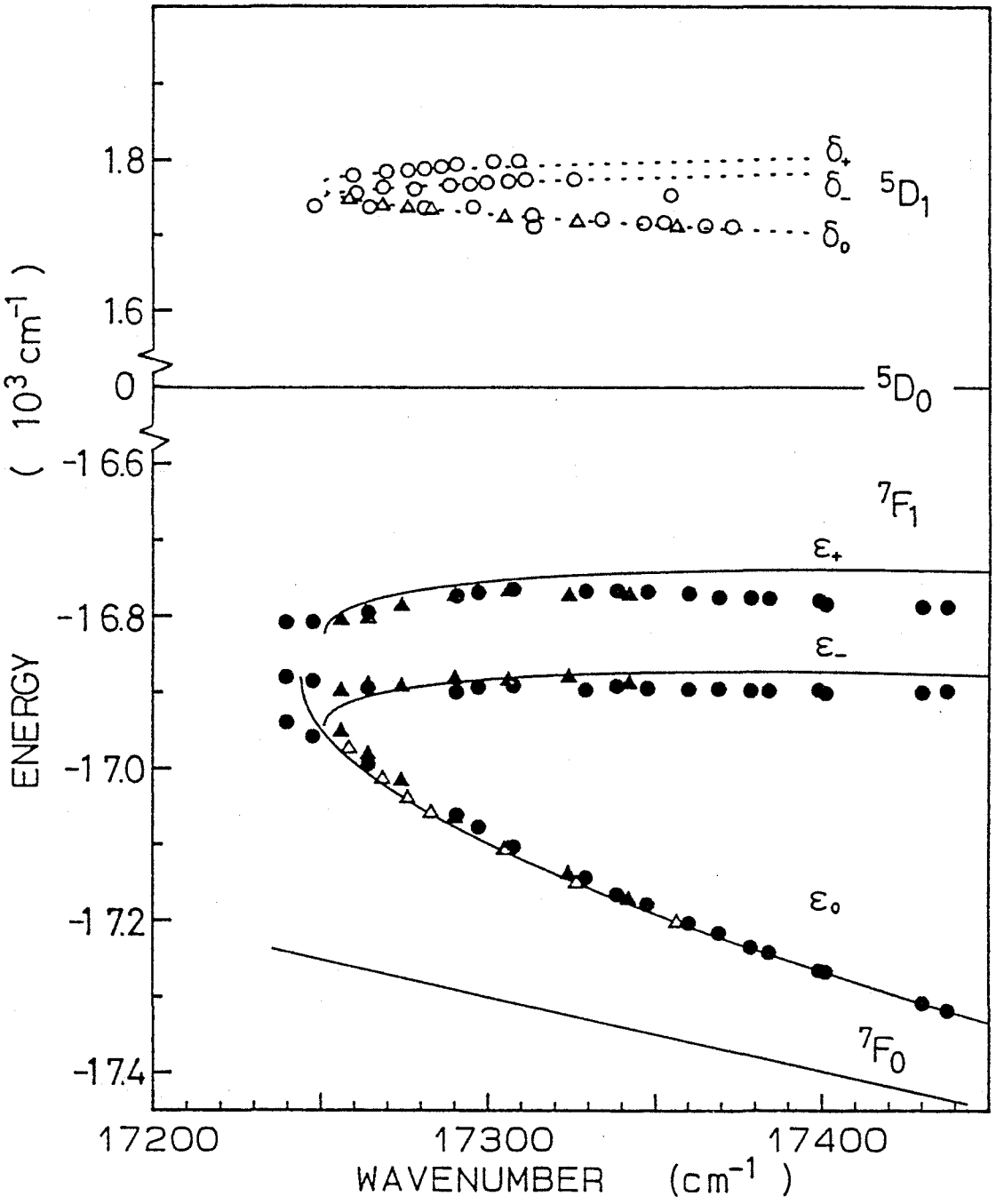

Figure 4.4: Energies of several levels of Eu^{3+} in $Ca(PO_3)_2$ glass relative to that of $^5D_0$ as a function of the $^5D_0$–$^7F_0$ energy separation. The closed circles, open circles, closed triangles and open triangles were determined from the fluorescence data under the $^7F_0$–$^5D_0$, $^7F_0$–$^5D_1$, $^7F_1(\varepsilon_0)$–$^5D_0$ and $^7F_1(\varepsilon_0)$–$^5D_1$ excitations, respectively. The solid lines show the fitting with Eqs.(5-2),(2-16) and (2-17). The dashed lines show the fitting with Eqs.(5-3)–(5-5).

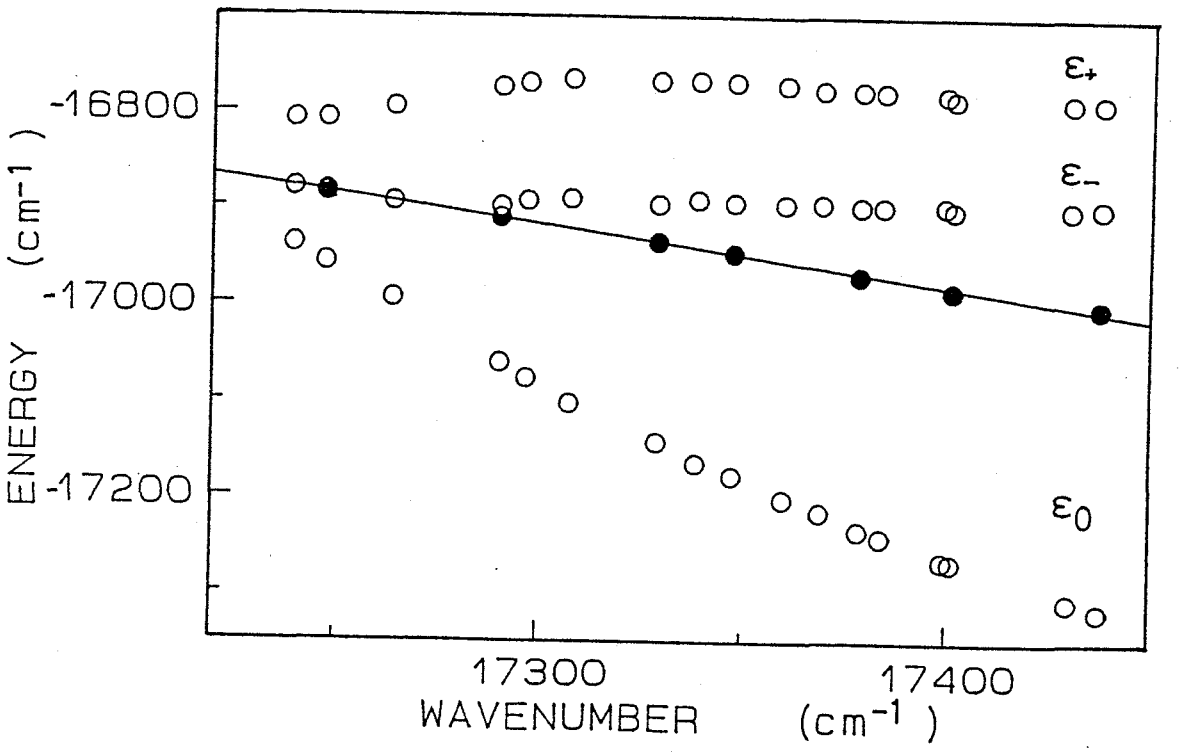

Figure 4.5: Energies of the $^7F_1$ manifolds of Eu^{3+} in $Ca(PO_3)_2$ glass relative to that of $^5D_0$ as a function of the $^5D_0$–$^7F_0$ energy separation. The open circles were determined from the fluorescence data for the $^7F_0$–$^5D_0$ excitation. The closed circles show the mean energy of the three $^5D_0$–$^7F_1$ lines. The solid line shows the fitting straight line determined for the center of gravity of the energy of the $^5D_0$–$^7F_1$ lines.

4.3 The Intensity of the Narrowed Fluorescence Spectra

As shown in Fig.4.2 (d), the intensity of the $^5D_0$–$^7F_0$ line relative to the $^5D_0$–ε_0 line decreases when the excitation energy is decreased. The intensity ratio of the $^5D_0$–$^7F_0$ to the $^5D_0$–ε_0 emission under the ε_0–δ_0 excitation is shown by open circles in Fig.4.6 as a function of the $^5D_0$–$^7F_0$ energy separation. The intensities of these lines were determined by integrating the high-energy sides of the peaks of these lines, because the contribution of other fluorescence components is negligible in these energy regions. As shown by a solid line in Fig.4.6, there exists a linear relation between the fluorescence intensity ratio and the energy of the site-selected $^5D_0$–$^7F_0$ line. On the other hand, the integrated intensity ratio of the $^5D_0$–$^7F_2$ to $^5D_0$–ε_+ emission under the ε_0–$^5D_0$ excitation, which is shown by open circles, is almost insensitive to the $^5D_0$–$^7F_0$ energy separation, as shown by closed circles in Fig.4.6.

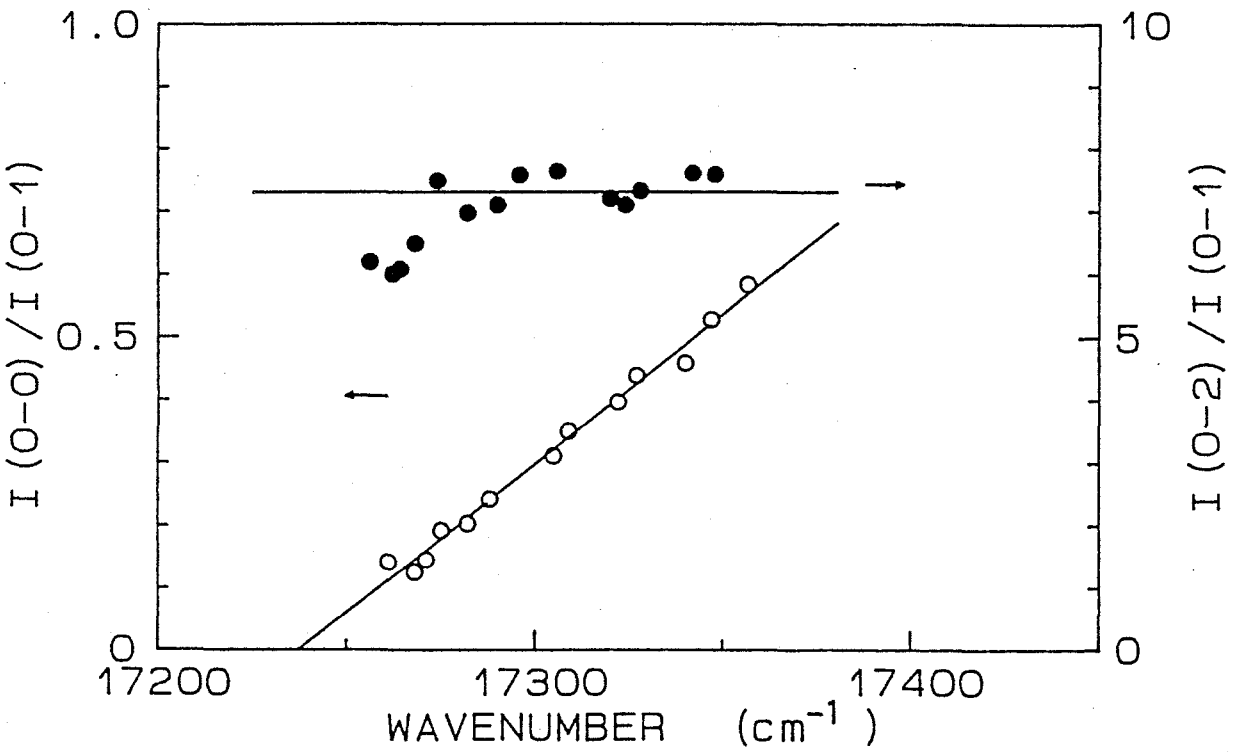

Figure 4.6: The open circles show the intensity ratio of the $^5D_0$–$^7F_0$ to the $^5D_0$–$^7F_1(\varepsilon_0)$ fluorescence line as a function of the site-selected $^7F_0$–$^5D_0$ transition energy under excitation into the $^5D_1(\delta_0)$ level. The closed circles show that of the $^5D_0$–$^7F_2$ to the $^5D_0$–$^7F_1(\varepsilon_+)$ fluorescence line under excitation into the $^7F_1(\varepsilon_0)$–$^5D_0$ line.

4.4 The Linewidth of the Narrowed Fluorescence Spectra

The linewidth of the $^5D_0$–ε_0 emission is rather insensitive to the excitation energy. However, the linewidth of this line was found to change with the absorption line to excite. As an example, the emission spectra of the $^5D_0$-ε_0 line under the $^7F_0$–$^5D_0$ and ε_0–$^5D_1$ excitations are shown in Fig.4.7. The linewidth of the $^5D_0$–ε_0 line under the ε_0–$^5D_1$ excitation is much narrower than that under the $^7F_0$–$^5D_0$ excitation. The HWHM obtained from high-energy side of the $^5D_0$–ε_0 line was about 18, 18 and 5 cm^{-1} for the $^7F_0$–$^5D_0$, $^7F_0$–δ_0 and ε_0–δ_0 excitations, respectively. On the other hand, the width of $^5D_0$–$^7F_0$ emission line was almost the same for the $^7F_0$–δ_0 (6 cm^{-1}), ε_0–$^5D_0$ (9 cm^{-1}) and ε_0–δ_0 (9 cm^{-1}) excitations. These results and calculated values using Eq.(5-13) are summarized in Table 4.1. This difference in linewidth is explained by the correlation between the energy of the transition of the absorption and the observed emission for the crystal field acting on the Eu^{3+} ions in resonance. We discuss this problem in Sec.5.3.

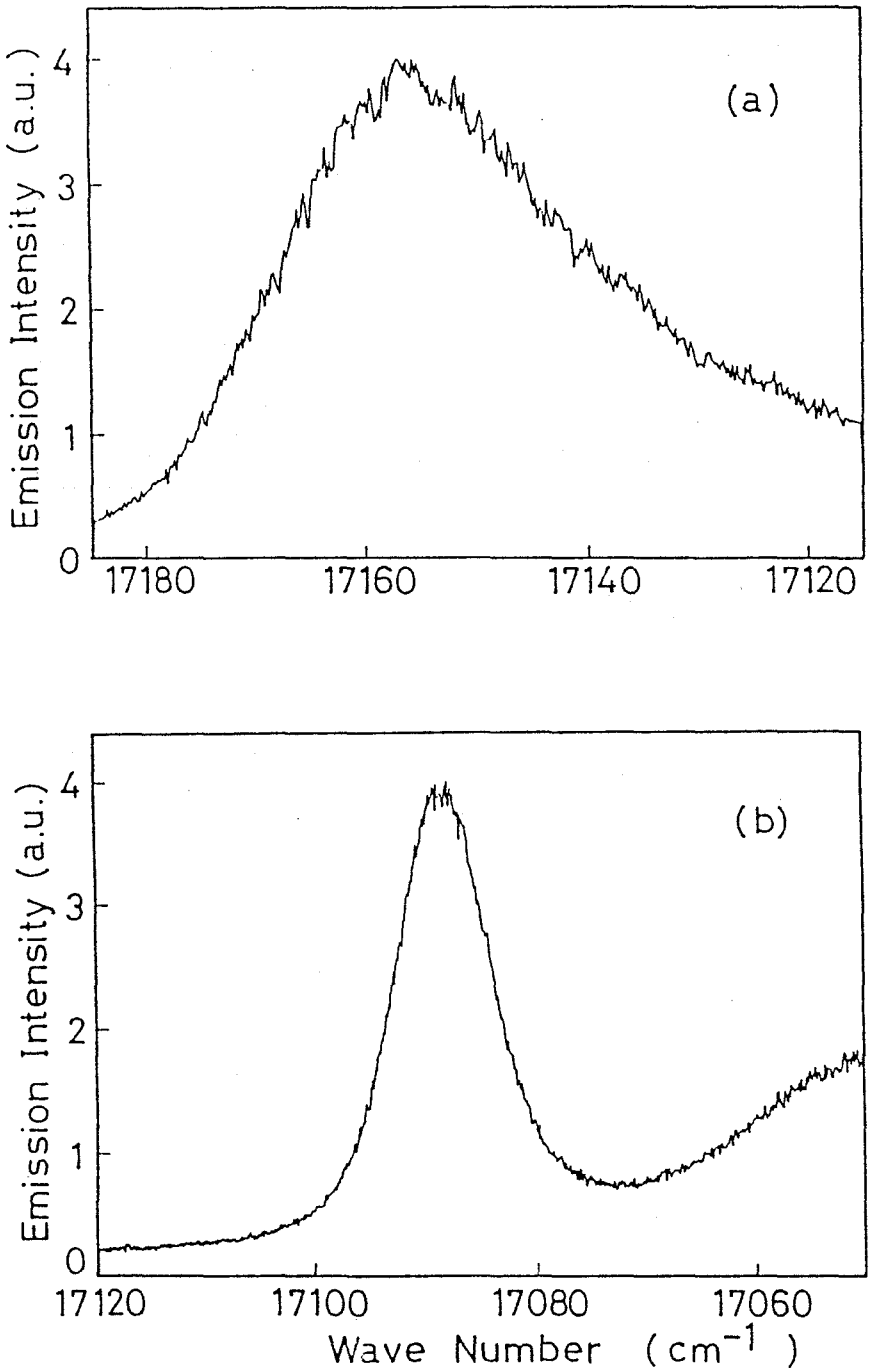

Figure 4.7: Fluorescence spectra due to the $^5D_0$–ε_0 transition under the excitation within the $^7F_0$–$^5D_0$ line; (a) , and the ε_0–δ_0 line; (b).

Transition			Linewidth (HWHM cm^{-1})	
excitation	emission	(energy cm^{-1})	experiment	calculation
$^7F_0$–$^5D_0$	$^5D_0$–ε_0	(17142)	18	8
ε_0–$^5D_0$	$^5D_0$–$^7F_0$	(17306)	9	5
$^7F_0$–δ_0	$^5D_0$–$^7F_0$	(17368)	6	2
	$^5D_0$–ε_0	(17200)	18	10
$^7F_0$–δ_-	$^5D_0$–$^7F_0$	(17306)	13	10
	$^5D_0$–ε_0	(17094)	24	11
ε_0–δ_0	$^5D_0$–$^7F_0$	(17329)	9	4
	$^5D_0$–ε_0	(17149)	5	1

Table 4.1: The linewidth of several emission lines obtained by the measurement under the monochromatic light excitation at 77K and the linewidth calculated by Eq.(5-13). The standard deviation of the distribution of Y employed is 240 cm^{-1}. The energy in the parentheses is the peak energy of the emission line.

4.5 The Polarization Characteristics of the Narrowed Fluorescence Spectra

We also studied the polarization characteristics of the $^5D_0$–$^7F_0$ and $^5D_0$–$^7F_1$ fluorescence lines under the linearly polarized light excitation into the $^7F_0$–$^5D_1$ and ε_0–$^5D_1$ absorption lines. The exciting light was directed in the x-direction and the component with the electric vector parallel to the z axis was selected by a Gran-Taylor prism. The polarization of the emission was analyzed by a Polaroid film, and a polarization scrambler was inserted between the analyzer and the entrance slit of the monochromator. Let us denote the intensity of the emission component with the electric vector parallel to the y-axis observed in the x-direction as Ixy. Table.4.2 shows the intensity ratios for the several transitions which are the mean of the experimental data. In the resonance fluorescence case, the polarization memory is considerably retained[KuTa 76]. In the present experiment, the polarization memory is lost by about 10% by the scattering due to the inhomogeneity of our sample and

Excitation	Emission	Ixy/Ixz	Iyx/Iyz	Izx/Izy
$^7F_0$–$^5D_1(\delta_0)$	$^5D_0$–$^7F_0$	0.99 ± 0.08	0.95 ± 0.25	0.84 ± 0.13
	$^5D_0$–$^7F_1(\varepsilon_0)$	0.64 ± 0.24	0.95 ± 0.21	1.69 ± 0.20
$^7F_0$–$^5D_1(\delta_\pm)$	$^5D_0$–$^7F_0$	0.92 ± 0.06	0.86 ± 0.17	0.92 ± 0.19
	$^5D_0$–$^7F_1(\varepsilon_0)$	1.42 ± 0.37	1.05 ± 0.14	0.79 ± 0.09
$^7F_1(\varepsilon_0)$–$^5D_1(\delta_0)$	$^5D_0$–$^7F_0$	0.55 ± 0.20	0.58 ± 0.12	0.98 ± 0.12
	$^5D_0$–$^7F_1(\varepsilon_0)$	1.08 ± 0.24	1.18 ± 0.19	1.10 ± 0.12
$^7F_1(\varepsilon_0)$–$^5D_1(\delta_\pm)$	$^5D_0$–$^7F_0$	1.13 ± 0.19	0.97 ± 0.12	0.94 ± 0.07
	$^5D_0$–$^7F_1(\varepsilon_0)$	1.12 ± 0.16	1.10 ± 0.08	1.03 ± 0.12

Table 4.2: The polarization characteristics of the $^5D_0$–$^7F_0$, $^7F_1(\varepsilon_0)$ fluorescence lines of $Ca(PO_3)_2$:Eu^{3+} under linearly polarized monochromatic light excitation into the $^7F_0$–$^5D_1$ and the $^7F_1(\varepsilon_0)$–$^5D_1$ absorption bands at 77K.

Transition	Iyx/Iyz	Izx/Izy
$^7F_0$–$^5D_0$	0.51	1.1
$^7F_1(\varepsilon_0)$–$^5D_0$	1.1	2.1
$^7F_2$–$^5D_0$	0.61	1.2

Table 4.3: Polarization characteristics obtained by the resonance fluorescence experiment of $Ca(PO_3)_2$:Eu^{3+} at room temperature [KuTa 76].

the cryostat windows. However, the polarization memory was considerably smaller for the non-resonant case than the resonance case. The polarization memory was retained only for the ($^7F_0$–δ_0 ;$^5D_0$–ε_0), ($^7F_0$–$\delta_\pm$;$^5D_0$–ε_0) and (ε_0–δ_0 ;$^5D_0$–$^7F_0$) lines, and the memory was almost lost for other lines.

5 Discussions

5.1 Polarization Characteristics and Line Assignment

If we consider the transition dipole is the same for the absorption and the emission lines, we expect $Ixy/Ixz < 1$, $Iyx/Iyz < 1$ and $Izx/Izy = 1$ when the transition is electric dipole in character, while $Ixy/Ixz < 1$, $Iyx/Iyz = 1$ and $Izx/Izy > 1$ when it is magnetic dipole. Using these polarization characteristics, the $^5D_0$–$^7F_0$ and $^5D_0$–$^7F_2$ line have already been identified as the electric dipole transitions and the $^5D_0$–$^7F_1$ as the magnetic dipole transition in $Ca(PO_3)_2$:Eu^{3+}[KuTa 76]. For the same reason with the experimental data in Table.4.2, the ε_0–δ_0 is assigned to the electric dipole transition, and $^7F_0$–δ_0 and $^7F_0$–$\delta_\pm$ lines to the magnetic dipole transitions. These assignments are consistent with the selection rules by the theoretical expectation. On the other hand, the selection rules for the $^7F_0$–$\delta_\pm$ transitions are considered to be different from that of the $^5D_0$–ε_0 transition while that of the $^7F_0$–δ_0 transition is considered to be the same from the polarization characteristics of the ($^7F_0$–$^5D_1$; $^5D_0$–ε_0) excitation-emission cycle in Table.4.2. This means that the irreducible representation of the point group of the Eu site to which the eigenfunctions of the $\delta_\pm$ levels belong is different from the representation which the eigenfunctions of the ε_0 and δ_0 levels belong to. Further, from the polarization characteristics of the ($^7F_0$–$^5D_0$; $^5D_0$–$^7F_1$) experiment [KuTa 76], it is suggested that the eigenfunctions of the $\varepsilon_\pm$ levels also belong to the different representation from that of the ε_0 level. Therefore, the ε_0 and δ_0 levels belong to the same representation which is different from that of the $\varepsilon_\pm$ and $\delta_\pm$ levels. These polarization characteristics are consistent with the observation that the $^5D_0$–ε_+ and $^5D_0$–ε_- transitions are similar to each other but are different from $^5D_0$–ε_0 in the laser-induced fluorescence line-narrowing characteristics as well as in the energy dependence in Fig.4.4.

Since the $^5D_0$–$^7F_{0,2}$ fluorescence lines due to the electric dipole transition are rather intense, it is clear that the Eu site has no inversion symmetry in this material. Further, the J degeneracy is completely removed for the $^7F_1$ and $^5D_1$ manifolds. Therefore, the point symmetry of the Eu site in $Ca(PO_3)_2$ glass is restricted to C_S, C_2, C_{2V} and D_2. If the $^5D_0$–$^7F_0$ transition is allowed due to the mixing of the other states by the even- or odd- parity crystal field potential, the transition dipole moment must contain A-representation of the point group of the Eu^{3+} site. In D_2 symmetry , z, x and y, and Lz, Lx and Ly transform like B_1,B_2 and B_3 representations, respectively. Therefore, the possibility of D_2 symmetry is excluded. The possibility of C_1 symmetry is also excluded on account of the presence of the clear polarization characteristics as mentioned before. Since the Eu^{3+} site in a monoclinic Eu_2O_3 crystal has C_S symmetry at high temperatures, several authors consider that the point symmetry of the Eu^{3+} site in oxide glasses is C_S [RiDe 69, ReVe 71]. If it is assumed that the point symmetry of the Eu^{3+} site is C_S, the $^5D_0$–$^7F_0$ line is allowed only for the x, y-component of the electric dipole vector. In this case, it is expected that the degree of polarization of the $^5D_0$–$^7F_0$ line for the $^7F_0$–$^5D_0$ excitation is much smaller than the experimental values in Table.4.3. Therefore, we conclude that the site symmetry of Eu^{3+} is C_2 or C_{2V}. This site symmetry agrees with that of the Yb^{3+} site in phosphate glass [RoFo 70].

If the Eu^{3+} ions are in various local environments and the excitation is made into the $^7F_0$–$^5D_1$ absorption band, they are considered to be excited equally because the magnetic dipole transition occurs irrespective of the presence or absence of the inversion symmetry. However, the emission lines which are not explained by the energy diagram of Fig.4.4 were not observed under the $^7F_0$–$^5D_1$ excitation. This fact, together with the smooth energy variation of all the levels in Fig.4.4, which means that the crystal-field strength changes continuously, suggests that every Eu^{3+} ion occupies the same kind of site restricted to C_2 or C_{2V} with different local field in this glass.

In the C_2 or C_{2V} symmetries, the $^7F_1$ and $^5D_1$ manifolds are split into three

energy levels. These eigenfunctions belong to the irreducible representations (A, B, B) or $(A_2,\ B_1,\ B_2)$. Because the selection rule of the $^5D_0$–ε_0 and $^7F_0$-δ_0 lines is different from that of the $^5D_0$–$\varepsilon_\pm$ and $^7F_0$–$\delta_\pm$ lines, the eigenfunctions of $\varepsilon_\pm$ and $\delta_\pm$ levels belong to the B (or B_1 and B_2) representation, and those of the ε_0 and δ_0 levels belong to the A or A_2 representation. These assignments mean that the ε_0 state corresponds to Ψ_1 while $\varepsilon_\pm$ to Ψ_2 and Ψ_3 of Eqs.(2-9)–(2-11).

The degree of polarization of the $^5D_0$–$^7F_0$ fluorescence in the direction of the excitation beam $[Ixz-Ixy]/[Ixz+Ixy]$ was about 0.5, when the excitation was made into the $^7F_0$–$^5D_0$ absorption band[KuTa 76]. This can be explained under the assumption that the direction of the C_2 or C_{2V} axis is random for each Eu^{3+} ion. In these point symmetries, the $^5D_0$–$^7F_0$ transition is allowed only for the electric field vector of light parallel to the direction of the C_2 or C_{2V} axis. However, when the excitation is made into the $^7F_0, \varepsilon_0$–$^5D_1$ band, the degree of polarization of the emission lines is small compared with the resonance experiment. $[Ixz - Ixy]/[Ixz + Ixy]$ was only about 0.25 for ($^7F_0$–δ_0 ;$^5D_0$–ε_0) and (ε_0–δ_0 ;$^5D_0$–$^7F_0$), which are considered to use the same dipole moment for the absorption and the emission transition, while was nearly zero for the other excitation-emission case. One of the causes of the small polarization memory is the memory loss due to the energy transfer effect. The phonon-assisted energy transfer does not contribute much to this effect at low temperatures because the sites diffuse mainly via the phonon emission and the excitation can not return to the sites selected by the excitation light. However, since the resonant transfer contributes to both of the site diffusion and returning process, this transfer mechanism is considered to reduce the polarization memory. The Eu^{3+} concentration of the sample employed is higher than that of the sample for the resonant experiment. Therefore, the energy transfer is considered to be not negligible in the present case.

The conclusion of this section is that the transitions of the $^7F_0$–$^5D_0, \varepsilon_0$–$^5D_0$, $^7F_0$–δ_0 and ε_0–δ_0 are determined to be the electric, magnetic, magnetic and

electric dipole transitions, respectively. The site symmetry of the Eu^{3+} ion in this glass is almost restricted to C_2 or C_{2V}. The C_2 or C_{2V} axis distributes randomly. The three Stark levels of the $^7F_1$ manifold are assigned to (A, B, B) or (A_2, B_1 or B_2) in order of increasing energy, and the similar assignment can be made for the $^5D_1$ manifold.

5.2 The $^5D_0$–$^7F_0$ Transition Mechanism

The $^5D_0$–$^7F_1$ transition probability is considered to be independent of the crystal-field strength, because the $^5D_0$–$^7F_1$ emission is due to the allowed magnetic dipole transition. Therefore, the result in Fig.4.6. indicates that the transition energy and the transition probability of the $^5D_0$–$^7F_0$ line are linearly correlated with each other. This can be explained by the mixing of other states into $^7F_0$ and $^5D_0$ due to the local-field perturbation, because both the energy shift and the probability of the optical transition induced by the mixing of levels with different energies are proportional to the square of the mixing coefficient of the wave function. It should be noted that both mechanisms of the forbidden $^5D_0$–$^7F_0$ transition discussed in Chap.2 are consistent with the result in Fig.4.6, because the above statement holds irrespective of whether the level mixing is due to the even- or odd- term of the crystal-field potential.

When there exist second-order terms of the crystal-field potential, the J-degeneracy is removed for the $^7F_1$ manifold. In this case, the energy splitting of Stark levels of the $^7F_1$ manifold is almost linearly proportional to the strength of the second-order term of the crystal-field potential. as mentioned before. The energies of these states are also affected by the spin-orbit coupling. However the strength of the spin-orbit coupling is insensitive to the crystal-field strength. Then, we neglect the spin-orbit coupling and only consider the level mixing through the crystal-field potential. As mentioned in Chap.2, there are two possible mechanisms of the level mixing between the $^7F_0$ state and the other states. One is the level mixing due to the even terms of the crystal-field potential and the other is due to the odd terms. If the energy shift of the $^7F_0$ is determined mainly by the odd terms of the crystal-field potential, in order to explain the quadratic relation between the energies of the $^7F_0$ and the ε_0 states and also the fact that the intensity ratio of the $^5D_0$–$^7F_2$ line to the $^5D_0$–ε_0 line is almost independent of the $^7F_0$–$^5D_0$ energy separation, we must assume the following. Namely, the strength of the odd term of the crystal-field potential

concerned with the $^5D_0$–$^7F_0$ transition and also with the pushed-down effect of the $^7F_0$ state, is proportional to the second-order term which determines the Stark splitting of the $^7F_1$ manifold. Further, the contribution of the linear term to the $^5D_0$–$^7F_2$ transition is negligible compared with that of the third-order term. However, these assumptions are not probable. On the other hand, if the site-to-site variation of the second-order term of the crystal-field potential is the dominant cause of the spreads of the energy and transition probability of the $^5D_0$–$^7F_0$ line, the quadratic relation and the intensity ratio of the $^5D_0$–$^7F_2$ to the $^5D_0$–$^7F_0$ are explained well. Therefore, we conclude that the spreads of energy and transition probability of the $^5D_0$–$^7F_0$ line in Fig.4.6 are not due to the effect of the variation of the odd-parity terms but due to that of the second-order term. Then, the dominant mechanism of the $^5D_0$–$^7F_0$ transition must be borrowing of intensity from the other lines through the J-mixing. In this case, the most important contribution comes from the mixing of $^7F_2$ into $^7F_0$ through $V_c^{(2)}$, as mentioned in Chap.2. Therefore, in the following, we examine if our experimental data can be explained by the site-to-site variation of the second-order term of the local-field potential.

The $^7F_2$ level mixes into $^7F_0$ not only through $B_{20}C_0^{(2)}$ term but also through $B_{2\pm2}C_{\pm2}^{(2)}$ terms of the local-field potential. Therefore, the contribution of the Y parameter to the transition probability of the $^5D_0$–$^7F_0$ line should be taken into account. However, from the linear relation between the energy and the intensity of the $^5D_0$–$^7F_0$ line under the ε_0–δ_0 excitation, the Y contribution is considered to be negligible, because in this case, the energy of the laser-induced fluorescence line is almost determined only by the X parameter. Therefore, the intensity and the energy of the $^5D_0$–$^7F_0$ line are approximately proportional to the value of X^2.

Because the $^5D_0$–$^7F_0$ transition is due to the J-mixing, we can estimate the intensity ratio of the $^5D_0$–$^7F_0$ line to the $^5D_0$–$^7F_2(M_J = 0)$ line under the monochromatic light excitation. As in Chap.2, if only the mixing through the

X parameter is considered, this intensity ratio is given by

$$r = [|< {}^7F_0| V_0^{(2)} |{}^7F_2\, M_J = 0>| / (E_0({}^7F_0) - E_0({}^7F_2))]^2$$
$$= \alpha X^2 / \Delta_{20} = -\Delta E_{00} / \Delta_{20} , \qquad (5\text{-}1)$$

where ΔE_{00} is the energy shift of the ${}^5D_0$–${}^7F_0$ line relative to the energy at $X = 0$, and Δ_{20} is the energy separation between the ${}^7F_0$ and the ${}^7F_2$ states. At $E_{00} = -17343$ cm^{-1}, the intensity ratio of the ${}^5D_0$–${}^7F_0$ line to the total intensity of the ${}^5D_0$–${}^7F_2$ lines is obtained as 0.02 ± 0.005 by the integration of the fluorescence spectra under the ε_0–${}^5D_0$ excitation. On the other hand, in this case, ΔE_{00} is estimated to be about $1 \cdot 10^2$ cm^{-1} ($E_{00}^0 = -17244$ cm^{-1} which is the energy separation between ${}^7F_0$ and ${}^5D_0$ at $V_c^{(2)} = 0$ referred from the fitting by Eq.(5-2), as in the following paragraph) and Δ_{20} is about $9.2 \cdot 10^2$ cm^{-1}. Then, we obtain r as about 0.11. If the intensities of the five lines of the ${}^5D_0$–${}^7F_2$ transition are assumed to be nearly equal. The intensity ratio of the ${}^5D_0$–${}^7F_0$ line to the total intensity of the ${}^5D_0$–${}^7F_2$ lines is estimated at 0.02, which is in good agreement with the measured value. This result indicates that the contribution of the mixing of the ${}^5D_0$–${}^7F_2$ transition through the Y parameter is very small, because the measured intensity of the ${}^5D_0$–${}^7F_0$ emission is expected to be much larger if the Y contribution is not negligible. Therefore, we conclude that the ${}^5D_0$–${}^7F_0$ transition is due to the borrowing of the intensity from the ${}^5D_0$–${}^7F_2(M_J = 0)$ through the axial second-order crystal-field potential in $Ca(PO_3)_2$:Eu^{3+}.

Next, we attempt to fit the energy variation in Fig.4.4 using Eqs.(2-15)–(2-17). The energies of the ${}^5D_0$ and ${}^5D_1$ states may be expressed using X and Y similarly as in Eqs.(2-15)–(2-18). However, the calculation is complicated because the Russell-Saunders approximation is not well applicable to ${}^5D$ states. Fortunately, because the energy separations between the ${}^5D$ states are larger than those between ${}^7F$ states, and also because the absolute value of the reduced matrix element $|< f^6\, {}^5D \,\|\, U^{(2)} \,\|\, f^6\, {}^5D >|$ is smaller than $|< f^6\, {}^7F \,\|\, U^{(2)} \,\|\, f^6\, {}^7F >|$, it is expected that the energy variation induced by

$V_c^{(2)}$ is much smaller for the $^5D_{0,1}$ states than for the $^7F_{0,1}$ states. This is consistent with our observation that the crystal-field splitting and also its dependence on the $^5D_0$–$^7F_0$ energy separation are much smaller for $^5D_1$ than for $^7F_1$ as seen in Fig.4.4. Therefore, it is considered to be a good approximation to assume that the energy of the $^5D_0$ state is independent of $V_c^{(2)}$. Hereafter, we employ this assumption.

In Fig.4.4, the energy variation of the $^5D_0$–$^7F_0$ line is dependent almost quadratically on that of the $^5D_0$–ε_0 line. Therefore, we assume that the energies $E(^7F_0)$ and $E(\varepsilon_0)$ are determined mainly by the axial symmetry parameter X. Then, regarding Y as a constant, we obtain the relation between the energy of the site-selected $^5D_0$–ε_0 line E_{01} and that of the $^5D_0$–$^7F_0$ line E_{00} as

$$E_{01} - E_{01}^* = a(E_{00} - E_{00}^*)^{1/2} + b(E_{00} - E_{00}^*) \,, \tag{5-2}$$

where $a = -\sqrt{3\Delta_{20}}/2$, $b = 9\Delta_{20}/14\Delta_{31}$, and E^* is the energy at $X = 0$. The solid line for the ε_0 level in Fig.4.4 shows the fitting curve derived from this relation with the experimentally obtained energies for the ε_0–δ_0 and ε_0–$^5D_0$ excitations. We see that the experimental data point are reproduced well by Eq.(5-2). The coefficients a and b were calculated from the energies of the ^7F_J states which were estimated from the peak energies of the $^5D_0$–$^7F_2$ (16327 cm^{-1}) and $^5D_0$–$^7F_3$ (15267 cm^{-1}) fluorescence lines under the excitation by the 465.8 nm Ar^+ laser line, while E_{01}^* and E_{00}^* were treated as adjustable parameters. From the best fit of the data for the ε_0–$^5D_1$ excitation, E_{01}^* and E_{00}^* were determined to be -17244 and -16882 cm^{-1}, respectively.

From the above fitting, we can say that the value of X changes between 0 and -1600 cm^{-1}, when the energy of the $^5D_0$–$^7F_0$ line changes between 17244 and 17400 cm^{-1}. In this energy range, it can be shown that the last terms in the right hand side of Eqs.(2-16) and (2-17) are smaller than the absolute values of the terms $\pm\sqrt{6}Y/10$. Then, the energy difference between the ε_+ and ε_- levels is given approximately by $\sqrt{6}Y/5$, and increases slightly as $|X|$ increases. In Fig.4.4, the ε_+–ε_- energy separation is almost constant,

and increases slightly as the energy of the $^5D_0$–$^7F_0$ line increases. This result supports the validity of our assumption that the value of Y does not change when that of X and accordingly the energy of the $^5D_0$–$^7F_0$ line vary. This means that the values of the parameters X and Y are not correlated with each other. From the energy separation between the ε_+ and ε_- states, the mean value of Y is determined to be about 240 cm^{-1}. The energies of the $^5D_0$–$\varepsilon_\pm$ lines calculated through Eqs.(2-16) and (2-17) with the same parameter values as before and Y = 240 cm^{-1} are also shown by solid lines in Fig.4.4. The agreement between the experiment for the ε_0–$^5D_0$ excitation and calculation is fairly good. The slight discrepancy may come from the fact that the $^5D_0$–$\varepsilon_\pm$ fluorescence lines are rather broad and also that the broad fluorescence due to the energy transfer overlap the site-selected spectrum.

Therefore, our assumption that the energies of the $^7F_0$ and ε_0 levels are almost determined by X while those of the $\varepsilon_\pm$ levels are determined by Y, which is independent of X, is good for the ε_0–$^5D_0$ and ε_0–$^5D_1$ excitations. On the other hand, the data points under the $^7F_0$–$^5D_0$ excitation are discrepant to those under the ε_0–$^5D_0$ excitation when the energy of the $^5D_0$–$^7F_0$ line is small as in Fig.4.4. It is also observed that the energy separation between the $\varepsilon_\pm$ levels is smaller and the energy of ε_0 level is larger for the $^7F_0$–$^5D_0$ excitation than for the ε_0–$^5D_0$ excitation when the energy of the $^5D_0$–$^7F_0$ is small. This is explained by the difference in the contribution of the Y parameter to the energies between the $^7F_0$ and the ε_0 levels. Namely, the Y contribution to the energy of the $^7F_0$ is not negligible compared with the X contribution while the Y contribution to the ε_0 level is negligible. The value of Y is estimated to be distributed between 0 and about 510 cm^{-1}from the width of the $^5D_0$–ε_+ line as will be discussed later. Then, the value of the term which contains Y is much smaller than the linear term of X in Eq.(2-15). Therefore, the energy of the ε_0–$^5D_0$ is determined almost solely by the X parameter, particularly, when the energy shift of ε_0 is large. However, the Y parameter largely contributes to the energy of the $^7F_0$–$^5D_0$ line, because the linear term of X is absent in Eq.(2-18).

Thus, when the excitation energy decreases within the $^7F_0$–$^5D_0$ line, Y also decreases. Therefore, the energy separation between the $\varepsilon_\pm$ levels, which is sensitive to Y as seen in Eqs.(2-16) and (2-17), decreases when the excitation energy decreases within the $^7F_0$–$^5D_0$ line. Then, the observed energies of the $\varepsilon_\pm$ levels under the $^7F_0$–$^5D_0$ excitation are discrepant to those under the ε_0–$^5D_0$,$^5D_1$ excitations.

On the other hand, at high energy-side of the $^5D_0$–$^7F_0$ line, the energies of $\varepsilon_\pm$ under the $^7F_0$–$^5D_0$ excitation are almost same to those under the ε_0–$^5D_0$, $^5D_1$ excitation as in Fig.4.4. This is explained as follows. Since the range of the value of Y is narrower and the mean value of Y is smaller than those of X, Y can be regarded as a constant of about mean value of Y (= 240 cm^{-1}), when the excitation energy is large. Thus, the separation of the $\varepsilon_\pm$ levels is insensitive to the excitation energy and the energies of these levels are almost same for the different excitation lines at the high-energy side of the $^5D_0$–$^7F_0$ line. Further, the energy transfer is not negligible in our sample and the $^5D_0$–$\varepsilon_\pm$ line is broad. In the phonon-assisted energy transfer [MoSh 73], that due to the absorption of the phonon is dominant when the excitation energy is small. In our experiment, the rate of the phonon absorption process is small compared with that of the emission since the temperature 77K is rather low. Therefore, when the excitation energy is small, the energy transfer is not significant and the peak shift of the $^5D_0$–$\varepsilon_\pm$ emission is observed. However, when the excitation energy is large, the $^5D_0$–$\varepsilon_\pm$ emission is insensitive to the excitation energy and is similar to that under the broad band excitation since the energy transfer rate is not small.

As mentioned before, the Y contribution to the energy of the ε_0 level is small. Thus, the discrepancy between the energy of the ε_0 level with the $^7F_0$–$^5D_0$ excitation and that with the ε_0–$^5D_0$,$^5D_1$ excitation is small. However, for the $^7F_0$–$^5D_0$ excitation, since the value of Y also decreases with decreasing the energy of $^7F_0$–$^5D_0$, the energy of the $^7F_0$–$^5D_0$ line largely decreases compared with the case that Y is neglected. Therefore, the data points of the ε_0 level with

the $^7F_0$–$^5D_0$ excitation are low lying compared with those with the ε_0–$^5D_0$,$^5D_1$ excitation at the low energy side of $^7F_0$–$^5D_0$ as in Fig.4.4.

Next, we attempt to fit the energy variation of the Stark levels of $^5D_1$. The energy shift of these levels due to the mixing of other J states is estimated to be small compared with that of the $^7F_1$ levels, because the energy denominator in the mixing coefficient is large. Therefore, we neglect the J-mixing effect and consider only the Stark splitting due to the second-order crystal-field potential. Since the angular parts of the matrix elements within the $^5D_1$ manifold are similar to those of the $^7F_1$ manifold, the energies of the Stark levels of $^5D_1$ are considered to be determined similarly by the linear terms of X and Y. Then, the energies are obtained as

$$E(\delta_0) = E_0(^5D_1) + AX \ , \tag{5-3}$$

$$E(\delta_-) = E_0(^5D_1) - AX/2 - BY \ , \tag{5-4}$$

$$E(\delta_+) = E_0(^5D_1) - AX/2 + BY \ , \tag{5-5}$$

where A and B are proportionality coefficients. It should be possible to calculate the values of A and B using the wave-functions of Ofelt. However, since this calculation is complicated, we treat these values and $E_0(^5D_1)$ as fitting parameters. The dashed lines in Fig.4.4 show the result of the fitting using X obtained by Eqs.(5-2). Thus, we obtained $A = 0.0375, BY = 10.4$ cm^{-1} and $E_0(^5D_1) - E_0(^5D_0) = 1760$ cm^{-1}. In these fittings, we used the experimental data for the $^7F_0$–$^5D_1$ and the ε_0–$^5D_1$ excitations, because the energy of the $^5D_1$ manifold determined by the ε_0–$^5D_1$ excitation is almost the same as that determined by the $^7F_0$–$^5D_1$ excitation.

As in Fig.4.5, the barycenter of the three $^7F_1$ levels is linearly correlated with the energy of $^5D_0$–$^7F_0$. The slope of this linearly correlation obtained by straight-line fit and the linear correlation coefficient obtained by this fitting are shown in Table.5.1. Since the linear correlation coefficient is unity, the linearity of this correlation is found to be very good. The barycenter of the $^7F_1$ manifold is calculated from Eqs.(2-15)–(2-17) as

$$E_G = E_0(^7F_1) - (7\beta + 2\gamma)(X^2 + 2Y^2) \ . \tag{5-6}$$

Accordingly, using Eq.(2-18), the mean energy referred to $^5D_0$ of the three fluorescence lines due to the $^5D_0$–ε_0 and $\varepsilon_\pm$ transitions can be expressed as

$$E_{0G} = E^*_{0G} + c\,(E_{00} - E^*_{00}) \ , \tag{5-7}$$

where $c = (7\beta+2\gamma)/\alpha$. This explains the linear dependence of the mean energy of the $^5D_0$–$^7F_1$ transition on the energy of the $^5D_0$–$^7F_0$ line. The slope of the solid line in Fig.4.5 of 0.63 is in fair agreement with the calculated coefficient $c = 0.50$. However, the difference between the observed and calculated coefficients seems to be too large to be explained by the errors in the estimation of the energy separations $\Delta_{JJ'}$. This difference cannot be explained by the pushed-down effect of $^5D_0$ due to the mixing of the higher levels. The larger value of the observed slope might come from the mixing of other states such as even-parity CTS into the $^7F_0$ and $^7F_1$ states through $V^{(2)}_c$.

Brecher and Riseberg [BrRi 80] studied the laser-induced fluorescence spectra of Eu^{3+} in oxide and fluoride glasses and discussed a model for the behavior of the first coordination shell of a rare-earth ion in the glassy matrix. In this analysis, these authors considered only the crystal-field splitting within a manifold and did not take into account the J-mixing. The correction of the level energies due to the J-mixing is not large because the coefficients β and γ are very small. However, the fact that the relation Eq.(5-7) applies well for their experimental data, as shown in Table 5.1, indicates that the J-mixing plays a significant role also in other glasses.

From Eqs.(5-2) and (5-7), the value of E^*_{01} is smaller than that of E^*_{0G} by $4(\gamma-\beta)Y^2$. Since this difference amounts only to 0.8 cm^{-1}, the experimentally obtained E^*_{01} and E^*_{0G} should coincide with each other. The value of E^*_{0G} determined from the above fitting is -16881 cm^{-1}, which is in good agreement with $E^*_{01} = -16882$ cm^{-1} obtained from the analysis of our experimental data using Eq.(5-2).

Glass	Slope	Linear correlation coeff.
Ca : metaphosphate	0.63 ± 0.012	1.00
NaBaZn : silicate[a]	0.61 ± 0.014	1.00
KCaAl : fluoroberyllate[b]	0.45 ± 0.015	0.99

Table 5.1: The slope of the linearly correlation between the energy of the $^5D_0$–$^7F_0$ line and the barycenter of the $^5D_0$–$^7F_1$ lines obtained by straight line fit for various glasses. The linear correlation coefficients which indicate the linearity are also shown.

[a] From [BrRi 76].
[b] From [BrRi 80].

The conclusion of this section is that the dominant $^5D_0$–$^7F_0$ transition mechanism is to borrow intensity from the $^5D_0$–$^7F_2$ line through the J-mixing due to the second-order local-field potential. The energies of the $^7F_0$,$^7F_1$ levels are also explained well by the Stark splitting and J-mixing effect due to the second-order terms. We found linear dependence of the mean energy of the three fluorescence lines due to the $^5D_0$–$^7F_1$ transition on the energy of the $^5D_0$–$^7F_0$ line. The slope of the straight line of this relation is in fair agreement with that calculated by considering the J-mixing through the second-order term. The three Stark levels of the $^5D_1$ manifold are reproduced only by the Stark splitting. This means that the J-mixing give only a small contribution to the energies of the ^5D levels, and also that to treat the energy of the $^5D_0$ as constant for various crystal-field strength is a good approximation.

5.3 Linewidth of Laser-Induced Fluorescence Spectrum

If the excitation migration due to the energy transfer is negligible, the narrowed fluorescence spectrum in the resonance fluorescence experiment usually gives a homogeneous line shape, which is a Lorentzian shape as discussed in Sec.1.2. In the non-resonance florescence experiment, however, the narrowed spectrum is usually broad compared with the resonance fluorescence and does not give a homogeneous line shape. In fact, the linewidth ($\sim$ 70 cm^{-1}) of the nonresonant emission of $^5D_0$–ε_0 in $Ca(PO_3)_2$:Eu^{3+} is larger than the average of the widths for the resonant emission of $^5D_0$–$^7F_0$ and $^5D_0$–ε_0, and accordingly the line shape of that emission is not considered to be homogeneous [KuTa 75].

In a glassy host, many crystal-field parameters are not negligible because the site-symmetry of the rare-earth ions is rather low. Then, usually we must take into account more than one crystal-field parameters, when we calculate the energy level of rare-earth ions in a glassy host. Further, the values of these parameters usually distribute widely. Therefore, even if the excitation is made using monochromatic light, the values of the crystal-field parameters which correspond to excited ions vary widely site by site. Usually, the dependence of the energy on the crystal-field is different for different energy levels. Thus, if a non-resonant excitation-emission process is considered, the emission line is broad compared with the resonant case, since the energy levels concerned to the transitions are different. The spectrum gives an inhomogeneous line shape which indicates the difference of the crystal-field dependence between the absorption and emission lines.

For the Eu^{3+} ion in $Ca(PO_3)_2$ glass, the crystal-field-induced energy shift of the $^7F_0$, $^7F_1$ and $^5D_1$ levels are determined by the second-order crystal-field parameters X and Y, as mentioned in Sec.5.2. When the monochromatic light excitation is made into an absorption band due to the ^7F–^5D transition, the sites in resonance with the excitation light can be expressed by a curve on

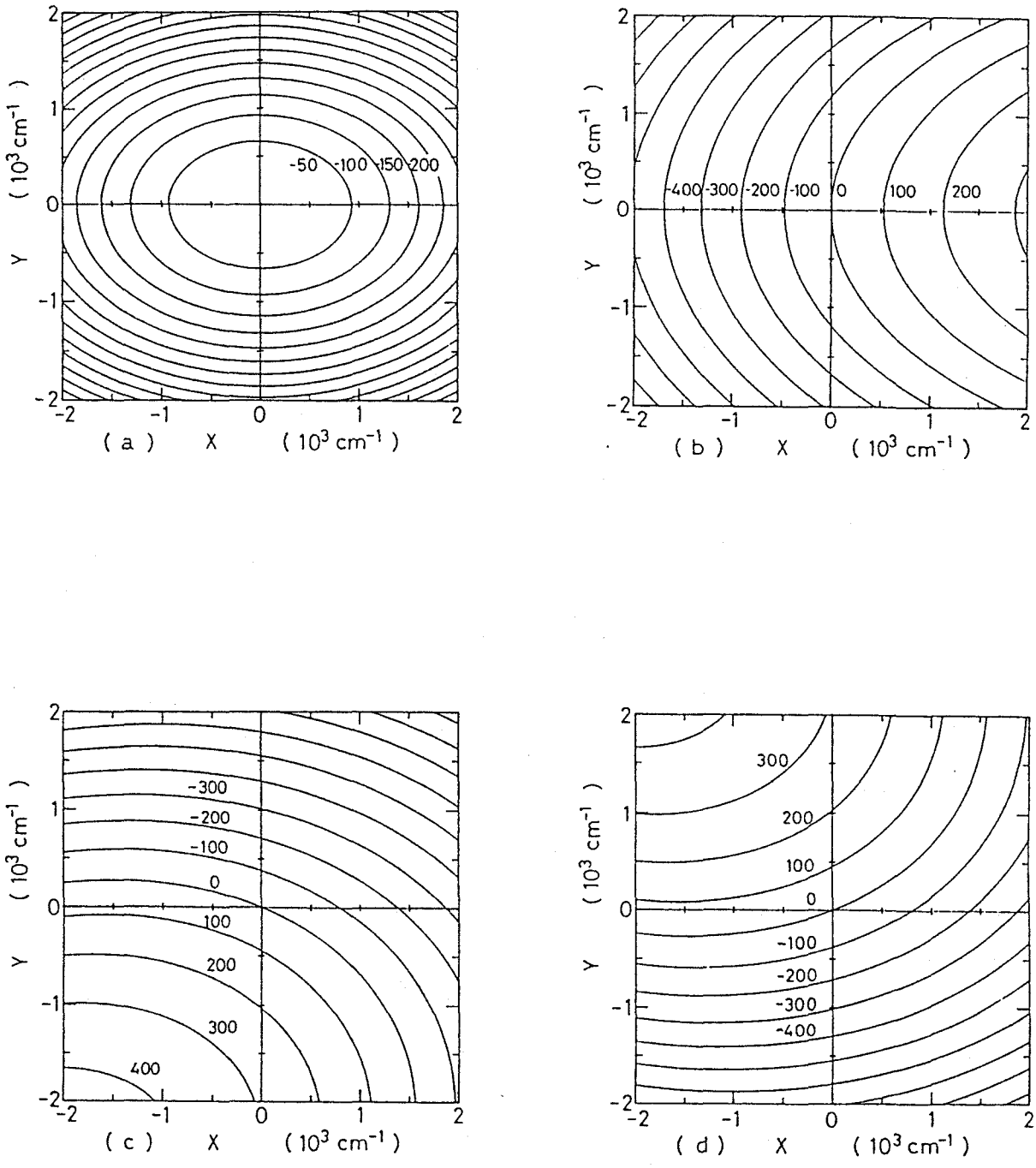

Figure 5.1: The contour line of the energy shift of the $^7F_0$ state (a), ε_0 state (b), ε_- state (c) and ε_+ state (d) on the $X - Y$ plane in the crystal-field parameters space. The step of the energy shift of line to line is 50 cm^{-1} for (a) and 100 cm^{-1} for (b)-(d).

the $X - Y$ plane in the crystal-field parameters space, as in Fig.5.1. The various sites in resonance correspond to the points on this curve. Namely, in Figs.5.1(a)–(d), the points on the solid lines show the various sites whose energy has the same value. Fig.5.1(a)–(d) show clearly the difference of the X and Y dependence of the ^7F levels. We notice that the energy of the ε_0 level is insensitive to Y, while the energies of the $\varepsilon_\pm$ levels are insensitive to X when the sites near the X axis are considered.

Now, let us consider a non-resonant excitation-emission cycle. For example, as in Fig.4.2, the $^5D_0$–$\varepsilon_\pm$ fluorescence lines are much broader than the $^5D_0$–$^7F_0$ and $^5D_0$–ε_0 lines, and this is insensitive to the excitation energy. This can be explained by the fact that the energies of the $\varepsilon_\pm$ states are sensitive to Y because of the terms $\pm\sqrt{6}Y/10$, while the energies of the $^7F_0$ and ε_0 states are insensitive to Y. Therefore, the broad spectral width of the $^5D_0$–$\varepsilon_\pm$ lines are almost attributed to the distribution of Y. If we assume that the energy of the ε_0–$^5D_0$ transition is independent of Y and the $^5D_0$–ε_+ energy variation is determined only through the term $\sqrt{6}Y/10$, we can estimate Y to range between 0 and 510 cm^{-1}, from the width of the low-energy side of the $^5D_0$–ε_+ fluorescence line (HWHM$\sim$ 65cm^{-1}). This value is rather small compared with that of $|X|$.

Next, we calculate the fluorescence line shape under monochromatic light excitation. We assume that the energy of the transition is determined by the two second-order crystal-field parameters X and Y and the phonon side band is negligible. If $\rho(X, Y)$ is the distribution function of crystal-field parameters X and Y for various sites, the distribution of excited states under the excitation with monochromatic light of energy E_L can be expressed as

$$f_{abs}(E_1, E_L)\, P_1(X, Y)\, \rho(X, Y)\ , \tag{5-8}$$

where E_1 is the center energy of the absorption line of the sites corresponding to a point (X, Y), P_1 is the probability of the transition of the absorption line and $f_{abs}(E_1, E_L)$ is the homogeneous line shape of the absorption line as in

Eq.(1-1). $P_1(X,Y)\rho(X,Y)$ is similar to $g(E_1)$ in Eq.(1-1). However, in this case, the energy of the transition is determined by two parameters X and Y. Therefore, the emission line shape is obtained by integrating Eq.(5-8) over X and Y. If we denote the emission energy as E_2 and the transition probability as P_2, the fluorescence line shape $F(E)$ is obtained as

$$F(E) = \iint dX dY \times f_{abs}(E_1, E_L)\, P_1(X,Y)\, \rho(X,Y)\, P_2(X,Y)\, f_{em}(E, E_2)\ , \tag{5-9}$$

where E is the energy of the observed emission and $f_{em}(E, E_2)$ is the homogeneous line shape. In our sample, since X and Y are not considered to be correlated with each other, the distribution function can be separated into two parts as

$$\rho(X,Y) = \rho_X(X)\, \rho_Y(Y)\ , \tag{5-10}$$

where ρ_X and ρ_Y are the distribution functions of the X and Y parameters, respectively. The distribution function is considered to be smooth with respect to X and Y because the observed spectrum is smooth. Further, it is considered to be a Gaussian-like function because each spectral line is reproduced by a Gaussian-like shape rather well under the deuterium lamp excitation.

If the homogeneous line shape functions f_{abs} and f_{em} are replaced by δ-functions, Eq.(5-9) can be integrated with respect to X and Y as

$$F(E) = \left|\frac{\partial(X\ ,Y\ )}{\partial(E_1, E_2)}\right|_{E_1=E_L\ ,E_2=E} \times P_1(X_0, Y_0)\, \rho_X(X_0)\, \rho_Y(Y_0)\, P_2(X_0, Y_0)\ , \tag{5-11}$$

where X_0 and Y_0 are the pair of the crystal-field parameters of the subset of the sites whose emission energy is E and the absorption energy is E_L. In other word, they are the coordinates of the crossing points between the two curves on the $X-Y$ plane determined by E_L and E. Here, $|\partial(X,Y)/\partial(E_1,E_2)|$ is a Jacobian. The assumption that f_{abs} and f_{em} can be treated as δ-function is probable for the case of ($^7F_0$–$^5D_0$; $^5D_0$–ε_0) and (ε_0–$^5D_0$; $^5D_0$–$^7F_0$) because the

homogeneous linewidths of ${}^5D_0$–${}^7F_0$ (< 0.5 cm^{-1}) and ${}^5D_0$–ε_0 (~ 5 cm^{-1}) at 77K are narrower than the inhomogeneous ones. However, when an emission spectrum concerned with the $\varepsilon_\pm$ levels is discussed, this approximation is not good.

When the energies of the absorption and the emission lines are expressed by the quadratic form of X and Y, the Jacobian diverges at the edges of the area which are near contact points between two curves corresponding to the absorption and emission lines, because the homogeneous line shapes are treated as δ-function. Since the linewidth can not be neglected where the Jacobian diverges, Eq.(5-11) is not a good approximation. If the area contributes considerably, the homogeneous line shape must be taken into account for the lineshape calculation. Here, we assume that the contribution of the area to the fluorescence spectrum is negligible and the Jacobian changes smoothly with E_L and E.

Using Eq.(5-11), we can evaluate the linewidth of the narrowed fluorescence of the Eu^{3+} ion under monochromatic light excitation. As in Sec.2.3 and Sec.5.2, the energies of the ${}^7F_0$,${}^7F_1$,${}^5D_0$ and ${}^5D_1$ states are expressed by a quadratic form of the X and Y parameters as

$$E_i = a_i X^2 + b_i X + c_i Y^2 + d_i Y + E_i^0 \ , \tag{5-12}$$

where E_i^0 is the energy in the case of $(X, Y) = (0, 0)$, and $i = 1$ and 2 denote the absorption line and the emission line, respectively. In Eq.(5-12), the crossing term of X and Y, which exists in the case of $d_i \neq 0$, is considered negligible because this term is small compared with the linear term of Y in our sample. If we take into account the crossing term, the equation becomes more complicated but the result does not change essentially. The coordinate (X_0, Y_0) on the $X - Y$ plane is calculated by solving two equations of Eq.(5-12) for $E_1 = E_L$ and $E_2 = E$.

The values of Y of the crossing points of Eqs.(5-12) for E_1 and E_2 are

obtained by eliminating X of Eqs.(5-12) as

$$r_c Y^2 + r_d Y \pm \frac{r_b}{2a_1}\sqrt{b_1^2 - 4a_1(c_1 Y^2 + d_1 Y + \Delta E_1)} + \Delta E_2 - \frac{a_2 \Delta E_1}{a_1} - \frac{b_1 r_b}{2a_1} = 0 \ , \qquad (5\text{-}13)$$

with

$$r_x = x_2 - \frac{a_2}{a_1} x_1 \ , \qquad \Delta E_i = e_i - E_i$$

where $x = b$,c or d. Y is obtained by solving Eq.(5-13), then X_0 is calculated using Eq.(5-12) and the emission spectrum is obtained. However, since this calculation is complicated, we calculate the width of the emission line with several assumptions. First, the Jacobian in Eq.(5-11) is assumed as a constant. As mentioned above, the Jacobian diverges at the contact points of two curves corresponding to the absorption and emission lines. However, except this points, this term is considered to change slightly with E because it is not probable that the value of the Jacobian, which contains at most the terms such as the inverse of the square root of the quadratic equation of E, varies violently. The assumption to take the Jacobian as a constant may be good when the excitation energy is large, because the contribution of the points where the Jacobian diverges is considered negligible in this case. However, when the excitation energy decreases, since the variable range of X and Y decreases and the contribution of the crossing points is not negligible, the assumption is not good. Second, X is regarded almost constant at the points of the curves determined by the energies of the $^7F_0$ and ε_0 near the Y axis. If the mean value and the variation of Y are small compared with those of X, the sites selected by the excitation light distribute near the Y axis. Then, X is regarded almost constant and the distribution of Y contributes more to the spectral shape of the emission line than that of X. In this case, the line shape is almost determined by the distribution of Y. As in Sec.5.2, the mean value of $Y(\sim 240\ \mathrm{cm}^{-1})$ is considerably small compared with that of X. However,

the variation of Y is not always considered small. Thus, this assumption may not be so good.

Under these assumptions, the line shape of the emission line is determined only by the variation of Y. Eq.(5-13) gives the energy of the emission line corresponding to the value of Y. Therefore, the linewidth of the emission line is estimated from the values of Y at the half maximum of the distribution of Y. As in Sec.5.2, the value of Y distributes between 0 to 510 cm^{-1} and the mean value of Y nearly equals to 240 cm^{-1}. Using these values, the linewidth (HWHM) of the emission line of $^5D_0$–ε_0 under the $^7F_0$–$^5D_0$ excitation is evaluated as in Fig.5.2. The solid line denotes the linewidth of the high-energy side of the emission line, and the dashed line denotes that of the low-energy side. The linewidth of the low-energy side is always smaller than that of the high-energy side. The linewidth of the high-energy side observed by the experiment is also shown by open circles. The linewidth was obtained by fitting the emission line with a Gaussian shape. In this fitting, the line shape of the high-energy side of the spectrum near the peak is well reproduced. However, the line shape of the low-energy side is broadened compared with that of the high-energy side. The linewidth of the low-energy side, which is about 1.5 times larger than that of the high-energy side, is not obtained accurately because the low-energy side overlaps with the high-energy side of the $^5D_0$–ε_- line. Further, the tail of the high-energy side is discrepant to the Gaussian tail due to the energy transfer.

As in Fig.5.2, the theoretical curve of the linewidth of the high-energy side is always rather small compared with that of the experimental value and the discrepancy between these values increases as the excitation energy is lowered. This discrepancy is due to neglecting the homogeneous widths of the $^5D_0$–$^7F_0$ and ε_0 lines. At 77K, indeed, the value of the homogeneous width of the $^5D_0$–ε_0 line (FWHM$\sim$ 5cm^{-1}) is not negligible while that of the $^5D_0$–$^7F_0$ line (FWHM$<$ 0.05cm^{-1}) is negligible. Therefore, the calculated half widths should be approximately 2.5 cm^{-1} larger. From this consideration, the theoretical

width is in agreement with the experimental value rather well. The discrepancy at the low excitation energy comes from the fact that the above assumption is not good and this is consistent with our expectation. Further, in this sample, the energy transfer effect is not negligible. From the result of Motegi and Shionoya [MoSh 73], the fluorescence line is considered to be broadened with increasing the time after the excitation light. In our experiment, we employed cw laser light for the excitation. Thus, the fluorescence line in this experiment must be broadened. Therefore, the energy transfer effect should be taken into account for the calculation.

On the other hand, the theoretical linewidth of the low-energy side is larger than that of the high-energy side. This tendency agrees with the experimental result, as shown in Fig.4.7. However, the theoretical value for the high-energy side is too large. This is because the distribution of X is not considered in the calculation. If the distribution of X is taken into account, the linewidth of the fluorescence depends on the distributions of X and Y. In this case, the linewidth will increase or decrease with changing the mean values and the standard deviations of the distributions of X and Y. However, the standard deviation of the distribution of Y should be smaller than that employed for the above calculation ($\sim 240\text{cm}^{-1}$) because the lineshape function is expressed as a convolution of two Gaussian-like functions. Therefore, the accurate widths are obtained only by the calculation which takes account of the distributions of X and Y.

In other excitation-emission case, from the similar calculation, we can evaluate the linewidth. The results are summarized in Table.4.1. The calculated width is small compared with the experiment data in all cases. However, if the homogeneous width of the ${}^5D_0$–ε_0 line is considered, this result will be in good agreement with experimental value. Anyway, the tendency of the linewidth with the excitation-emission processes is well explained by this theory.

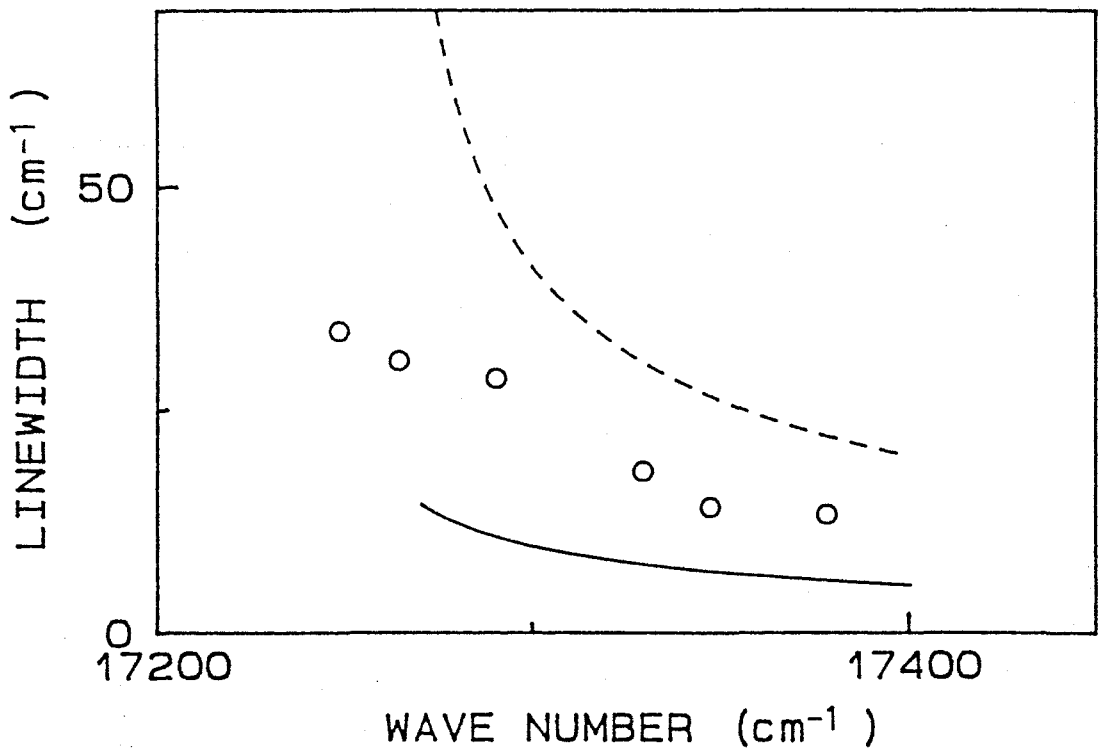

Figure 5.2: The width of the $^5D_0$–ε_0 line under the monochromatic light excitation into the $^7F_0$–$^5D_0$ absorption band at 77K as a function of excitation light energy. The solid and the dashed lines show the theoretical curves for the linewidths of the high-energy and the low-energy sides calculated by Eq.(5-13), respectively.

5.4 Inhomogeneously Broadened Line Shape of the $^5D_0$–$^7F_0$ Line

Fig.5.3 shows the fluorescence spectrum of $Ca(PO_3)_2$:Eu^{3+} excited by the UV light from a deuterium lamp through a visible cut filter. The spectrum is asymmetric with a longer tail in the high-energy side. Previously, it was reported that the crystal field mixing of a higher level to the $^7F_0$ state explains this asymmetric spectral shape[TaKu 79]. In this discussion, the transition probability of the $^5D_0$–$^7F_0$ line was taken to be independent of its energy, because it was tacitly assumed that this transition is allowed by the mixing of the odd-parity CTS while the $^7F_0$ state is pushed downwards by the mixing of $^7F_2$. However, since this was found to be not the case in Eu^{3+} in $Ca(PO_3)_2$, we shall extend the theoretical treatment of Ref.[TaKu 79] to incorporate the effect of the mixing on the transition probability[KuNi 88].

As described in Sec.2.3 and Sec.5.2, we found that transition probability and the energy of the $^5D_0$–$^7F_0$ line depend on X and on both X and Y, respectively. From these results, we can calculate the spectral shape of this inhomogeneously broadened line provided the distributions of the parameters X and Y are known. As in Sec.5.3, the spectral shape under the monochromatic light excitation is given by Eq.(5-9). Further, the line shape under the broad light excitation can be obtained as a convolution of Eq.(5-9) and the line shape of the excitation light. However, the spectral line shape can not be obtained by this kind of convolution calculation in the case of the UV excitation, because there are many absorption lines concerned with the transition of the Eu^{3+} ion in the UV spectral region. When the excitation light is very broad, Eu^{3+} in the various sites, in which the crystal-field strength is different from each other, are considered to be excited rather homogeneously. Then, we may be able to regard the line shape function of the excitation light, the transition probability P_1 and the homogeneous line shape function f_{abs} of the absorption lines as constants. The spontaneous emission probability is proportional to the

power of the emission energy. However, this factor is not considered in Sec.5.3, because the linewidth of the narrowed spectrum is narrow enough to consider the factor as a constant. Now, the E^4 factor is also taken into account. Then, the spectral shape $F(E)$ is obtained as

$$F(E) \propto \iint dX\,dY\; E^4 \delta(E_2 - E)\, P_2(X,Y)\rho(X,Y)\ . \tag{5-14}$$

When the emission of the $^5D_0$–$^7F_0$ line is considered, the transition probability and the energy of this line are dependent on the X and Y parameters. However, as in Sec.5.2, the transition probability is proportional to the square of X while is almost independent of Y in this sample. Therefore, we put P_2 and E_2 as

$$P_2(X,Y) \propto X^2\ ,$$

$$E_2 \equiv E_{00} = E_{00}^0 + \alpha\,(X^2 + 2Y^2)\ ,$$

where E_{00} is the energy of the $^5D_0$–$^7F_0$ line. Next, we assume that the distribution of X and Y is expressed by a product of two Gaussian distribution functions as

$$\rho(X,Y) = \frac{1}{\sqrt{2\pi\sigma_x^2}} \exp\left[-\frac{(X-X_m)^2}{2\sigma_x^2}\right] \frac{1}{\sqrt{2\pi\sigma_y^2}} \exp\left[-\frac{(Y-Y_m)^2}{2\sigma_y^2}\right]\ , \tag{5-15}$$

where σ_x and X_m are the standard deviation and the mean value of X, respectively, and σ_y and Y_m are those of Y. Finally, the fluorescence spectral shape for the broad band light excitation is obtained as

$$\begin{aligned} F(E) \propto E^4 \int dX \frac{\xi X^2}{\sqrt{1-\xi^2X^2}} \exp\left[-\frac{1}{2}\left(\frac{X-X_m}{\sigma_x}\right)^2\right] \\ \times \left\{\exp\left[-\frac{1}{2}\left(\frac{\sqrt{1-\xi^2X^2}-M_y}{\Sigma_y}\right)^2\right]\right. \\ \left. + \exp\left[-\frac{1}{2}\left(\frac{\sqrt{1-\xi^2X^2}+M_y}{\Sigma_y}\right)^2\right]\right\}\ , \end{aligned} \tag{5-16}$$

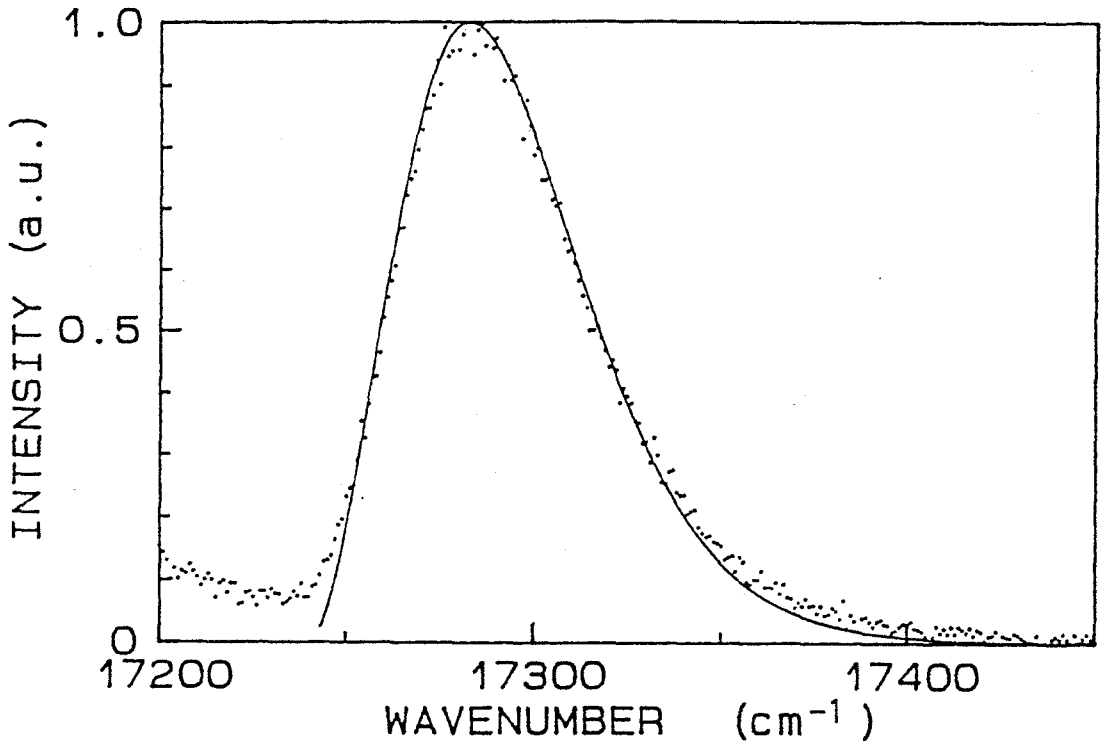

Figure 5.3: Fluorescence spectrum due to the $^5D_0$–$^7F_0$ transition in $Ca(PO_3)_2$:Eu^{3+} excited by a deuterium lamp at 77K. The solid line shows the theoretical curve derived from the relation (5-16).

with

$$\xi = \sqrt{\alpha/(E - E_{00}^0)} \ ,$$

$$M_y = \sqrt{2}\xi\, Y_m \ , \qquad \Sigma_y = \sqrt{2}\xi\, \sigma_y \ .$$

In fig.5.3, the experimental data are compared with Eq.(5-16). In this fitting, the following values have been employed and the integral has been calculated numerically with changing X_m and σ_x which are the fitting parameters: $Y_m = 240\text{cm}^{-1}$, $\sigma_y = 240\text{cm}^{-1}$, $E_{00}^0 = 17244\text{cm}^{-1}$ and $E_{02}^0 = 16327\text{cm}^{-1}$. From this calculation, the last term in the braces in the integral of Eq.(5-16) has been found to be negligible. As shown in Fig.5.3, the theoretical curve reproduces well the $^5D_0$–$^7F_0$ fluorescence spectrum at 77K under the broad UV light excitation. From this fitting, the mean value and the standard deviation of X have been determined as $X_m = -795\text{cm}^{-1}$ and $\sigma_x = 240\ \text{cm}^{-1}$.

The asymmetric spectral shape has also been observed for the $^5D_0$–$^7F_0$ transition of Eu^{3+} in other glasses[RiDe 69, ReVe 71, BrRi 76, BrRi 80]. Since the spectral shape is very similar to that in Fig.5.3, it is probable that the above explanation also applies to these cases.

The conclusion of this two sections is the following. The fluorescence lines for the non-resonant fluorescence-line narrowing experiment are usually inhomogeneously broadened. The linewidths of these broadened lines were found to change with the selection of the absorption lines in $Ca(PO_3)_2$:Eu^{3+}. This result is explained well by the X,Y-dependence of the energy separation of the concerned transition. Further, the linewidths of the fluorescence lines obtained by the calculation which only takes account of the distribution of Y are in agreement with those of the experiment rather well. On the other hand, the inhomogeneously broadened fluorescence of the $^5D_0$–$^7F_0$ line for the broad band UV light excitation has a long high-energy tail. This is explained by the fact that the energy and the probability of the $^5D_0$–$^7F_0$ transition are determined by the parameter of X and its magnitude distributes widely in this sample. The experimental data is also well reproduced by the theoretical fluorescence line shape, and the mean value and the standard deviation of X have been determined as –795 cm^{-1} and 240 cm^{-1}, respectively. Further, the distribution function of X has been found to be a Gaussian.

6 Conclusion

The laser-induced fluorescence-line narrowing experiment has been performed for the Eu^{3+} ion in $Ca(PO_3)_2$ glass. The energies and the intensities of the ${}^5D_0$–${}^7F_J$ transitions have been measured in detail for various excitation energies within the ${}^7F_0$,${}^7F_1$–${}^5D_0$,${}^5D_1$ absorption bands. The polarization characteristics of these fluorescence lines have been also studied.

From the polarization characteristics, the ${}^7F_0$–${}^5D_1$ line has been determined to be due to the magnetic dipole transition, while the ε_0–${}^5D_1$ line to the electric dipole transition. Since the ${}^7F_1$ manifold is fully split and the polarization memory of the fluorescence lines considerably remains, the site symmetry of the Eu^{3+} ions are restricted to C_S,C_2,C_{2V} and D_2. In the D_2 symmetry, the mechanism of the ${}^5D_0$–${}^7F_0$ transition is not explained because the transition dipole moment of ${}^5D_0$–${}^7F_0$ should contain A-representation of the point group. Thus, the D_2 symmetry is excluded. The degree of polarization of the ${}^5D_0$–${}^7F_0$ transition with the resonance excitation is explained by the random distribution of the direction of the axial transition dipole. This fact excludes the C_S symmetry of the Eu^{3+} site. Therefore, the site symmetry is determined to the C_2 or C_{2V}. The three Stark levels of the ${}^7F_1$ and ${}^5D_1$ manifolds are assigned to (A,B,B) or (A_2,B_1 or B_2) components in order of increasing energy. The fact that the degree of polarization of the ${}^5D_0$–${}^7F_0$ and ${}^5D_0$–ε_0 lines with the nonresonant excitation is rather small suggests that the energy transfer contributes the fluorescence lines.

The linear relation between the energy and the intensity of the ${}^5D_0$–${}^7F_0$ fluorescence line has been found, while the intensity of the ${}^5D_0$–${}^7F_2$ fluorescence is almost constant for various excitation energies. Further, the relation between the energy of the ${}^5D_0$–${}^7F_0$ line and that of the ${}^5D_0$–ε_0 line has been reproduced fairly well by the quadratic equation. Since the energy shift of the ${}^5D_0$–ε_0 line is almost determined by the axial component of the second-order term of the crystal-field potential, the energy shift of the ${}^5D_0$–${}^7F_0$ is concluded to

come from the J-mixing between $^7F_0$ and $^7F_2$ ($M_J = 0$) through this term. Therefore, the transition of the $^5D_0$–$^7F_0$ line is determined to be due to the borrowing of the intensity from the $^5D_0$–$^7F_2$ line through the J-mixing via the second-order crystal-field potential.

The energy levels of $^7F_1$ have been reproduced fairly well by the equations which take into account the Stark splitting and J-mixing effects, and those of $^5D_1$ have been also reproduced well by the Stark splitting. The linear relation between the energy of the barycenter of the three Stark levels of $^7F_1$ and that of $^7F_0$ have been explained well by the above energy level calculation.

The linewidth of the laser-induced fluorescence lines are explained well by the distribution of the second-order crystal-field parameters. The contribution of the energy transfer effect for the line broadening is suggested to be rather large. The fluorescence line shape of the $^5D_0$–$^7F_0$ line with the broad band excitation is reproduced well by the equation which takes into account the distributions of the second-order crystal-field parameters. From this fitting, the distribution functions of these parameters has been found to be well approximated by Gaussian functions.

References

[AlBa 77] O.K.Alimov, T.T.Basiev, Yu.K.Voron'ko, L.S.Gaĭgerova and A.V.Dmitryuk, Zh.Eksp.Teor.Fiz. **72**, 1313 (1977) [Sov.Phys. JETP **45**, 690 (1977)].

[AnHa 72] P.W.Anderson, B.I.Halperin and C.M.Varma, Phil. Mag. **25**, 1 (1972).

[AvCa 77] P.Avouris, A.Campion and M.A.El-Sayed, J.Chem.Phys. **67**, 3397 (1977).

[BiNe 70] S.S.Bishton and D.J.Newman, J.Phys.C: Solid St. Phys. **3**, 1753 (1970).

[BrRi 76] C.Brecher and L.A.Riseberg, Phys.Rev.B **13**, 81 (1976).

[BrRi 80] C.Brecher and L.A.Riseberg, Phys.Rev.B **21**, 2607 (1980).

[BrWe 80] S.A.Brawer and M.J.Weber, Phys.Rev.Lett. **45**, 460 (1980).

[Ch 63] N.C.Chang, J.Appl.Phys. **34**, 3500 (1963).

[CoSh 35] E.U.Condon and G.H.Shortley, *The Theory of Atomic Spectra*, Cambridge Univ.Press, (London and New York, 1953).

[CrCr 68] Hannah Crosswhite, H.M.Crosswhite and B.R.Judd, Phys.Rev. **174**, 89 (1968).

[Di 68] G.H.Dieke, *Spectra and Energy Levels of Rare Earth Ions in Crystals.*, (Wiley, New York, 1968).

[DeKi 67] Yu V.Denisov and V.A.Kizel, Opt.Spectrosc. **23**, 251 (1967).

[ElSt 53] R.J.Elliott and K.W.H.Stevens, Proc.Roy.Soc. **A219**, 387 (1953).

[ElJu 57] J.P.Elliott, B.R.Judd and W.A.Runciman, Proc.Roy.Soc. **A240**, 509 (1957).

[FeJa 69] M.S.Feld and A.Javan, Phys.Rev. **177**, 540 (1969).

[FrWa 62] A.J.Freeman and R.E.Watson, Phys.Rev. **127**, 2058 (1962).

[GaKu 65] P.K.Gallagher, C.R.Kurkjian and P.M.Bridenbaugh, Phys.Chem. Glasses **6**, 95 (1965).

[Go 74] A.A.Gorokhovskii, R.K.Kaarli and L.A.Rebane, Sov.Phys. JETP Lett **20**, 216 (1974).

[GrCo 61] J.B.Gruber and J.G.Conway, J.Chem.Phys. **34**, 632 (1961).

[HeYe 78] J.Hegarty, W.M.Yen and M.J.Weber, Phys.Rev.B **18**, 5816 (1978).

[HeBr 80] J.Hegarty, R.T.Brundage and W.M.Yen, Appl.Opt. **19**, 1889 (1980).

[HoIm 77] T.Hoshina, S.Imanaga and S.Yokono, J.Lumin. **15**, 455 (1977).

[JøPa 63] C.K.Jørgensen, R.Pappalardo and H.H.Schmidtke, J.Chem.Phys. **39**, 1422 (1963).

[JøPa 64] C.K.Jørgensen, R.Pappalardo and E.Rittershans, Z.Naturforsch **20a**, 54 (1964).

[Ju 59] B.R.Judd, Mol.Phys. **2**, 407 (1959).

[Ju 62] B.R.Judd, Phys.Rev. **127**, 750 (1962).

[Ju 66] B.R.Judd, Phys.Rev. **141**, 4 (1966).

[JuCr 68] B.R.Judd, H.M.Crosswhite and Hannah Crosswhite, Phys.Rev. **169**, 130 (1968).

[KuGa 63] C.R.Kurkjian, P.K.Gallagher, W.R.Sinclair and E.A.Sigety, Phys.Chem. Glasses **4**, 239 (1963).

[KuTa 75] T.Kushida and E.Takushi, Phys.Rev.B **12**, 824 (1975).

[KuTa 76] T.Kushida, E.Takushi and Y.Oka, J.Lumin. **12/13**, 723 (1976).

[KuNi 88] T.Kushida and G.Nishimura, J.Lumin. **40/41**, 111 (1988).

[MoCh 81] J.R.Morgan, E.P.Chock, W.D.Hopewell, M.A.El-Sayed and R.Orbach, J.Phys.Chem. **85**, 747 (1981).

[MoSh 73] N.Motegi and S.Shionoya, J.Lumin. **8**, 1 (1973).

[NiBl 66] W.C.Nieuwpoort and G.Blasse, Solid State Commun. **4**, 227 (1966).

[NiBl 67] W.C.Nieuwpoort, G.Blasse and A.Bril , in *Optical Properties of Ions in Crystals*, edited by H.M.Crosswhite and H.W.Moos (Interscience, New York, 1967), p.161.

[NiKo 64] C.W.Nielson and G.F.Koster, *Spectroscopic Coefficients for p^n,d^n, and f^n Configurations.*, MIT Press, Cambridge, Massachusetts, 1964.

[NiKu 88] G.Nishimura and T.Kushida, Phys.Rev.B **37**, 9075 (1988).

[Of 62] G.S.Ofelt, J.Chem.Phys. **37**, 511 (1962).

[Of 63] G.S.Ofelt, J.Chem.Phys. **38**, 2171 (1963).

[Ph 72] W.A.Phillips, J. Low Temp. Phys. **7**, 351 (1972).

[Ra 43] G.Racah, Phys.Rev. **63**, 367 (1943).

[Ra 49] G.Racah, Phys.Rev. **76**, 1352 (1949).

[RaWy 63] K.Rajnak and B.G.Wybourne, Phys.Rev. **132**, 280 (1963).

[Ri 61] E.C.Ridley, Proc. Cambridge Phil. Soc. **56**, 41 (1961).

[RiDe 69] D.K.Rice and L.G.DeShazer, Phys.Rev. **186**, 387 (1969).

[Ri 72a] L.A.Riseberg, Phys.Rev.Lett. **28**, 786 (1972).

[Ri 72b] L.A.Riseberg, Solid State Comun. **11**, 469 (1972).

[Ri 73] L.A.Riseberg, Phys.Rev.A **7**, 671 (1973).

[ReVe 71] R.Reisfeld, R.A.Velapoldi, L.Boehm and M.Ish-Shalom, J.Phys.Chem. **75**, 3980 (1971).

[Re 76] R.Reisfeld, Structure and Bonding **30**, 65 (1976).

[ReLi 76] R.Reisfeld, N.Lieblich, L.Boehm and B.Barnett, J.Lumin. **12/13**, 749 (1976).

[RoFo 70] C.C.Robinson and J.T.Fournier, J.Phys.Chem.Solids **31**, 895 (1970).

[SeHu 76] P.M.Selzer, D.L.Huber, D.S.Hamilton, W.M.Yen and M.J.Weber, Phys. Rev. Lett. **36**, 813 (1976).

[Se 81] P.M.Selzer, in *Laser Spectroscopy of Solids*, edited by W.M.Yen and P.M.Selzer (Springer-Verlag, Berlin, 1981), p.113.

[Sz 70] A.Szabo, Phys.Rev.Lett. **25**, 924 (1970).

[TaKu 79] E.Takushi and T.Kushida, J.Lumin. **18/19**, 661 (1979).

[To 39] R.Tomaschek, Trans. Faraday Soc. **35**, 148 (1939).

[Va 37] J.H.Van Vleck, J.Phys.Chem **41**, 67 (1937).

[WaFr 67] R.E.Watson and A.J.Freeman , Phys.Rev. **156**, 251 (1967).

[We 81] M.J.Weber, in *Laser Spectroscopy of Solids*, edited by W.M.Yen and P.M.Selzer (Springer-Verlag, Berlin, 1981), p.189.

[WeBr 82] M.J.Weber and S.A.Brawer, Journal de Physique *Colloque* **C9**, 291 (1982).

[Wy 61] B.G.Wybourne, J.Chem.Phys. **35**, 340 (1961).

[Wy 62] B.G.Wybourne, J.Chem.Phys. **36**, 2295 (1962).

[Wy 67] B.G.Wybourne, in *Optical Properties of Ions in Crystals*, edited by H.M.Crosswhite and H.W.Moos (Interscience, New York, 1967), p.35.

[Ye 86] W.M.Yen, in *Optical Spectroscopy of Glasses*, edited by I.Zschokke (Ridel, Holland, 1986), p.23.

Acknowledgments

The author wishes to express his sincere thanks to Prof.T.Kushida for suggesting this work, invaluable discussion and continuous encouragements.

He also acknowledges Prof.S.Saikan, Dr.M.Kimura, Dr.S.Kinoshita and Dr.A.Kurita for their valuable suggestions.

He is indebted to Prof.T.Eisei for providing all glasses used in this work.